

Style and timing of late Quaternary faulting on the Lake Edgar fault, southwest Tasmania, Australia: Implications for hazard assessment in intracratonic areas

Dan Clark*

Geohazards Division, Earthquake Hazard and Neotectonics Project, GPO Box 378, Canberra, ACT 2601, Australia

Matt Cupper*

Mike Sandiford*

School of Earth Sciences, The University of Melbourne, Melbourne, Victoria 3010, Australia

Kevin Kiernan*

School of Geography and Environmental Studies, University of Tasmania, Hobart, Tasmania 7001, Australia

ABSTRACT

Geomorphic analysis of the ~30-km-long Lake Edgar fault scarp in southwestern Tasmania suggests that three large surface-rupturing events with vertical displacements of 2.4 m to 3.1 m have occurred in late Quaternary time. Optically stimulated luminescence (OSL) age estimates from a sequence of three periglacial fluvial terraces associated with faulting constrain these events to ca. 18 ka, ca. 28 ka, and ca. 48–61 ka. A similar amount of vertical displacement during each faulting event suggests that surface-breaking earthquakes on this fault are characteristically of magnitude M_w 6.8–7.0. Estimates for the average slip rate calculated over two complete seismic cycles range from 0.11 to 0.24 mm/yr, which is large for a stable continental region fault. This sequence represents the first recurrence data for surface-rupturing earthquakes on an eastern Australian Quaternary fault, and one of only a few for the entire Australian continent.

INTRODUCTION

Quantitative seismotectonic and seismic hazard analysis of stable continental regions is hampered by an absence of good constraints on the recurrence intervals of large earthquakes, which are infrequent in these regions compared to plate-boundary

regions. Paleoseismological investigations provide the only viable avenue to obtain such constraints (e.g., Machette, 1998) in a useful time frame. The success of paleoseismological investigations has greatly increased with recent developments in Quaternary dating techniques for sedimentary deposits, such as thermoluminescence (TL) and particularly optically stimulated luminescence

*E-mails: dan.clark@gov.au; cupper@unimelb.edu.au; mikes@unimelb.edu.au; Kevin.Kiernan@utas.edu.au.

(OSL; e.g., Burbank and Anderson, 2000). In this paper, we use the OSL technique to constrain the timing of large earthquakes on the Lake Edgar fault in Tasmania, Australia (Fig. 1).

Australia is a relatively active stable continental region, with an estimated seismic-moment release of $\sim 9 \times 10^{23}$ dyn cm/yr (Johnson et al., 1994). The historical seismic record suggests that earthquakes of moment magnitude (M_w) 6.8 occur about once every 20–30 yr across the Australian continent. A longer record of large earthquakes is indicated by an abundance of surface-rupturing faults of presumed late Quaternary age (Crone et al., 1992, 1997, 2003; note that late Quaternary is taken to mean younger than marine isotope stage 5e, or younger than ca. 125 ka). Crone et al. (1997, 2003) obtained recurrence data for several of these surface-rupturing faults in Western Australia, South Australia, and the Northern Territory. These authors demonstrated episodic rupture characteristics on these faults with interseismic intervals of the order of 10 k.y. to 100 k.y.

A prior study of the Lake Edgar fault by McCue et al. (2003) provided evidence for multiple Quaternary surface-rupturing events but lacked firm time constraints. The objective of our new work is to obtain new dating control for the timing of the earthquakes. We begin by presenting the results of field mapping and dating of well-constrained sandy sediment samples. These data are then used to construct a history of Quaternary displacement on the Lake Edgar fault, from which significant insight into the behavior of intracratonic faults may be gained. The results therefore have particular bearing on seismic hazard assessments in Australia, and for intracratonic areas worldwide.

LAKE EDGAR FAULT AND ITS REGIONAL CONTEXT

Regional Geological Context and Pre-Quaternary History of Movement

The northerly trending, west-side-up Lake Edgar fault scarp lies on the boundary between the Adamsfield-Jubilee and Tyennan tectonic units (Fig. 1; see Seymour and Calver, 1995). The scarp marks the surface trace of the Lake Edgar fault, which has been mapped over a strike length of ~ 45 km (Turner et al., 1985; Seymour and Calver, 1995). The fault terminates to the north in the Adamsfield ultramafic complex and links into a southeasterly trending fault fronting the Arthur Range to the south.

Drilling prior to construction of the Edgar dam (Fig. 2) suggested that the fault dips $\sim 65^\circ$ – 70° west (Roberts et al., 1975). The fault is thought to have accommodated ~ 12 km of left-lateral displacement during the Paleozoic (Roberts et al., 1975; Calver et al., 1990). A narrow, possibly discontinuous, sliver of limestone has been dragged into the fault trace for a distance of 1.2 km south of the western Edgar dam abutment (Roberts et al., 1975).

The fault juxtaposes mudstone, siltstone, orthoquartzite, and carbonates of the Proterozoic Clark Group against mudstone, chert, sandstone, and conglomerates of the Cambrian Island Road Formation and Ragged Complex (Brown et al., 1995). Island Road Formation and Ragged Complex rocks are only present on

the western side of the fault, whereas Clark Group rocks are on both sides of the fault. The ranges to the east of the fault, which direct west-flowing drainage across the fault in the Lake Edgar region, are mainly composed of orthoquartzite. Large areas of Quaternary sediment are localized to the eastern side of the fault (Brown et al., 1995; Kiernan, 2001; Fig. 2) owing to east-side-down movement on the fault.

Regional Geomorphology and Evidence for Quaternary Deformation

The geomorphology of the region surrounding the Lake Edgar fault is dominated by processes and landforms relating to the Huon Plains, through which the scarp cuts, and the Mount Anne Massif, which lies to the east of the fault (Fig. 2). The vegetation consists of heathy shrubland and button grass plains (Figs. 3A–3C), with scrub and forest locally along drainage courses (Balmer and Corbett, 2001). Large-scale erosion, transportation, and deposition of coarse clastic sediment appear to have been very limited during the Holocene (Kiernan, 2001). The morphology of fans, which are prominent along the foot of the Mount Anne Massif, is the result of Pleistocene periglacial fluvial and alluvial sedimentation (Kiernan, 1990). These sediments are typically mantled by peat and organic-rich silt. Predam aerial photographs suggest that there has been a minor amount of lacustrine sedimentation within Lake Edgar and its companion lake (Kiernan, 2001; Fig. 4). Deposits and landforms relating to three or four distinct glaciations have been identified in the Lake Edgar region (Kiernan, 1990). The youngest is late Pleistocene (younger than 25 ka), whereas the oldest may be ca. 2 Ma in age. The intervening one or two glaciations are considered to be middle Pleistocene in age.

The Lake Edgar fault scarp was first recognized as the surface expression of a recently active fault by Carey and Newstead (1960). Periglacial fans emanating from the ranges to the east are clearly cut by the fault, both to the north (Figs. 3D, 3E, and 5) and south (Figs. 3A, 3B, and 6) of Edgar Dam. Variability in the fault's scarp height where it cuts the fan (2.5 m to 6 m; McCue et al., 2003, their figure 5) has been attributed to episodic incision of the scarp by fluvial processes. McCue et al. (2003) suggested that at least two surface-rupturing earthquake events, each resulting in ~ 2.5 m of west-side-up vertical displacement, had occurred in the Quaternary.

McCue et al.'s (2003) log of a trench excavated by the Hydro Electric Commission (Roberts et al., 1975) clearly shows the trace of the most recent faulting event in fan gravels inferred to be late Pleistocene in age. The fault plane dips steeply to the west (60° – 70°) but flattens toward the surface, becoming almost horizontal at its intersection with the ground surface. Folded dia-genetic (or postdepositional) quartz laminae in the silty strata beneath the fan gravels truncate against the contact with the overlying (overthrust) gravel sheet. This deformation and truncation of strata inferred to be initially horizontal were attributed to a penultimate event (McCue et al., 2003).

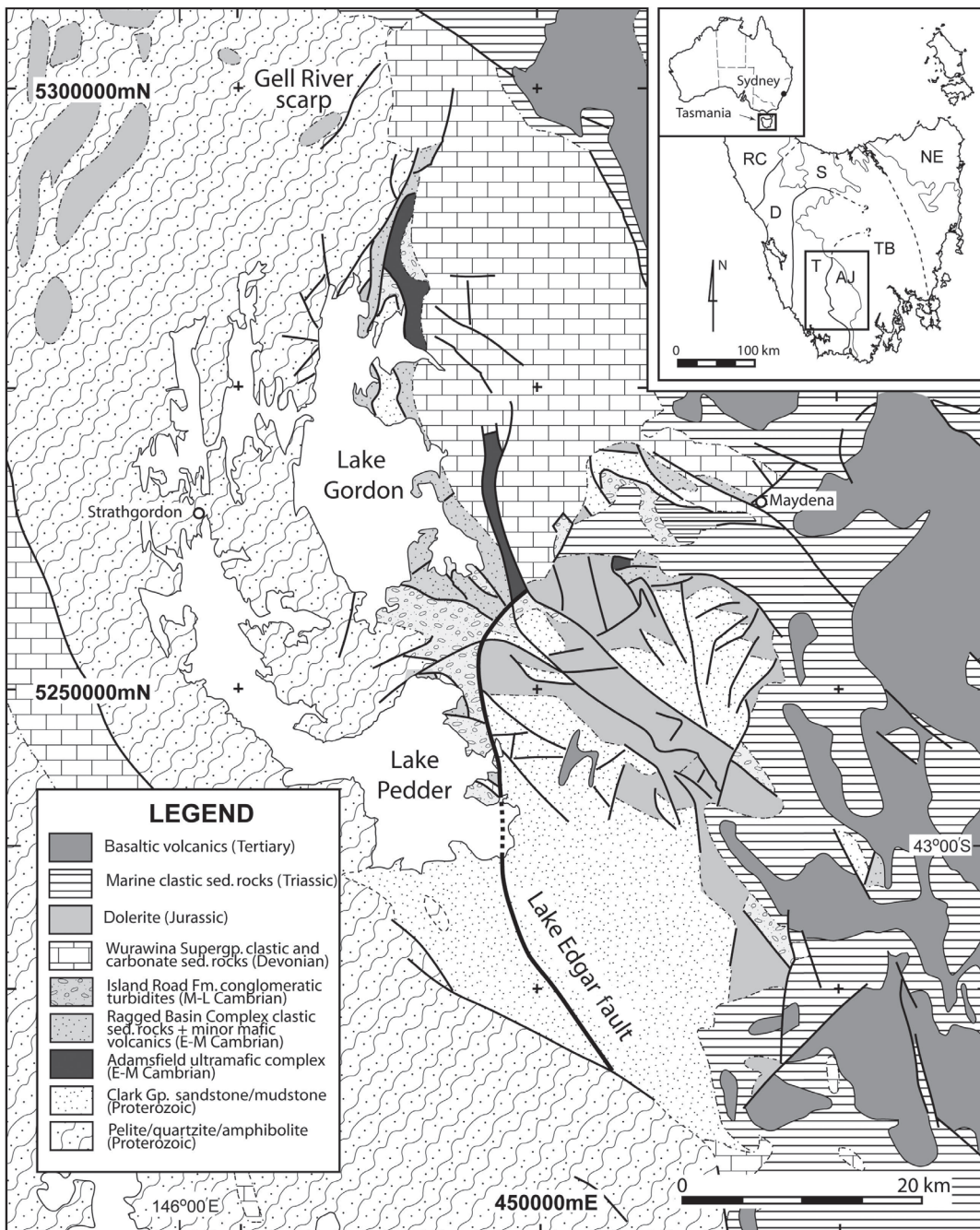


Figure 1. Location map and regional geology in the area of the Lake Edgar Fault (compiled from Brown et al., 1995; Kiernan, 2001; Seymour and Calver, 1995; Turner et al., 1985). Lithologic contacts are shown as dashed lines, while fault contacts are shown as solid lines. Lake Edgar fault is marked by a heavy line. Key to tectonic units: RC—Rocky Cape; D—Dundas; S—Sheffield; T—Tyennan; AJ—Adamsfield-Jubilee; NE—NE Tasmania; TB—Tasmania Basin.

Glacial outwash fans cut by the Lake Edgar fault have been interpreted to date from the early Pleistocene Eliza glacial stage (Kiernan, 1985, 1990). However, as mentioned already, McCue et al. (2003) suggested that the fault also truncates deposits relating to the most recent glaciation, but this was based upon

an earlier model (i.e., Carey and Newstead, 1960) that only recognized a single late last glacial stage glaciation in Tasmania. The younger of their two proposed events was inferred to have occurred subsequent to the Last Glacial Maximum (LGM; i.e., within the past 25,000 yr), based upon several lines of evidence.

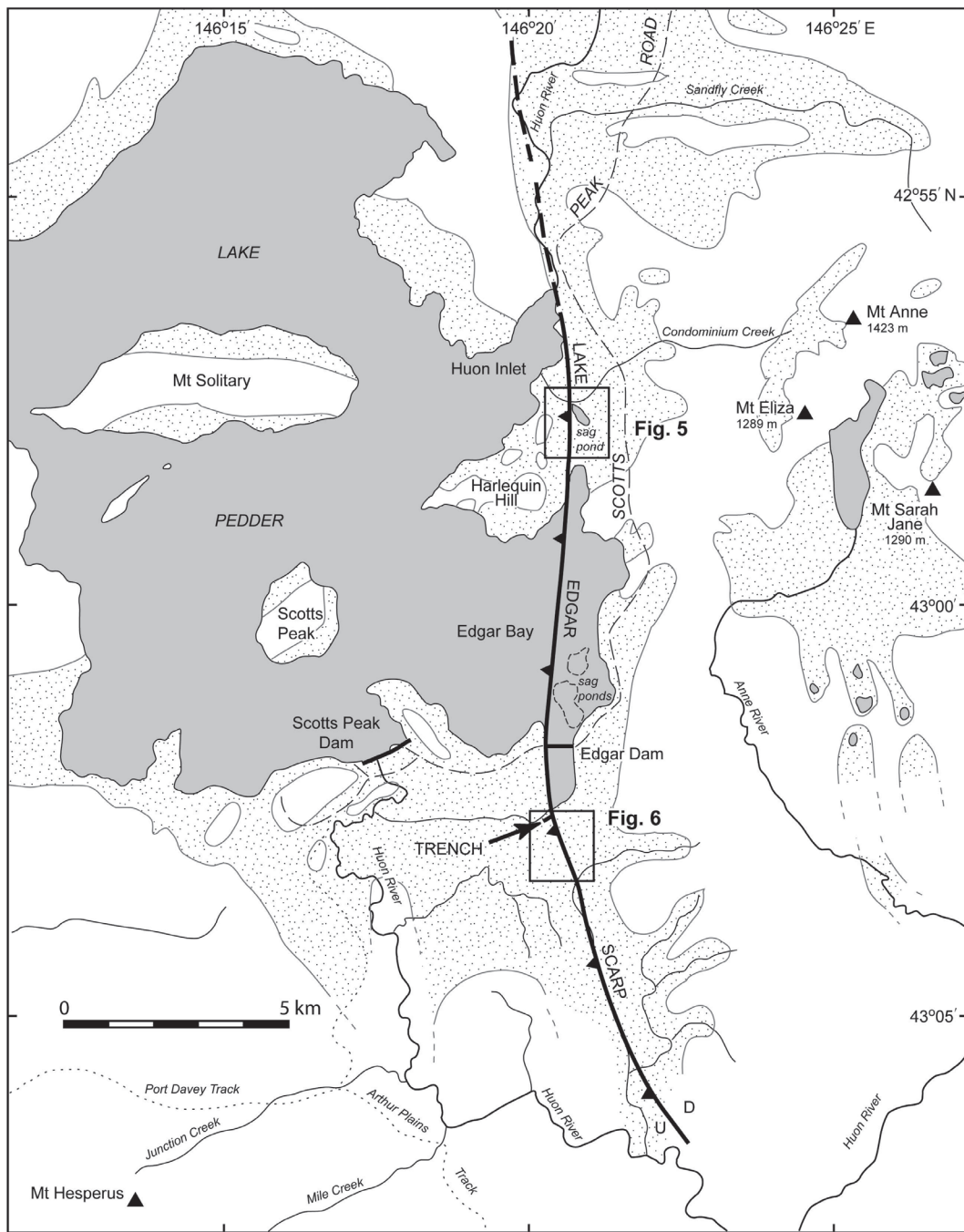


Figure 2. Map of the Lake Pedder area (gray pattern is permanent water) showing the location of the specific study sites mentioned in the text (modified after McCue et al., 2003). Areas of significant Quaternary sediment accumulation (>1 m) are shown by stipple pattern. Triangular ticks on the fault indicate westerly fault dip. The surface of Lake Pedder is ~310 m above mean sea level. Abbreviations for surface displacement: U—up; D—down.

First, the scarp is a very sharp and prominent feature in the landscape, significantly more so than scarps associated with several historic surface ruptures in Australia (e.g., Meckering—Clark and McCue, 2003; Tennant Creek—Crone et al., 1992). Second, geologically recent movement on the structure is inferred from

the observation that drainages ponded against the fault scarp have not yet been filled with sediment. This is despite the fact that southwest Tasmania receives ~2500 mm of rain annually (Carey and Newstead, 1960). Furthermore, the unweathered nature of the gravels displaced in the trench excavation contrasts

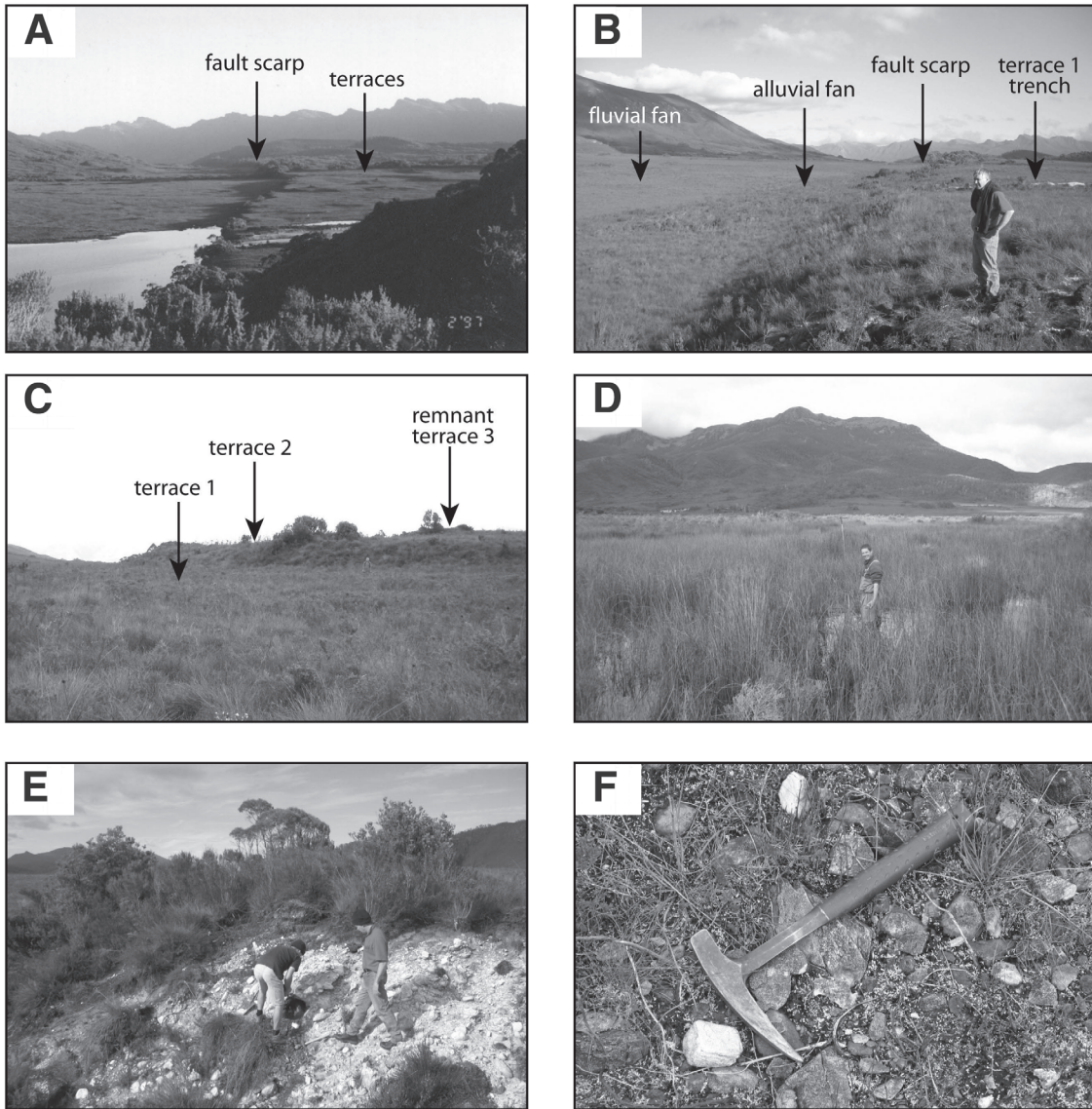


Figure 3. Series of photographs illustrating the geomorphology of the Lake Edgar fault scarp. (A) Fluvial fans south of Edgar dam (looking south along the fault scarp), (B) detail of terrace 1 (looking south along fault scarp), (C) detail of terrace 2 (looking south), (D) sag pond north of Harlequin Hill (looking east toward the Condominium Creek catchment), (E) scarp profile north of the sag pond (looking south along fault; location shown on Fig. 5), and (F) gravel on terrace 2, south of Edgar dam; 33 cm pick for scale. For A, field of view of the middle ground at the position of the arrows is ~4.2 km. There is a 1.8-m-tall person standing on the Terrace 1 bench (between the arrow heads) in C.

with the highly weathered gravels characteristic of Eliza glacial stage fans.

McCue et al. (2003) discussed a second fault scarp along the Gell River, some 50 km north of the Lake Edgar fault (Fig. 1). The Gell River scarp is shorter (~10 km long) and more subdued than the Lake Edgar scarp. This relationship was interpreted to reflect a greater time having elapsed since the last event on the Gell River scarp relative to the Lake Edgar scarp, although proof of fault movement has not been established, and preliminary field

observations suggest the possibility that the scarp could relate to the surface outcrop of a thin Permian gravel bed rather than to a fault (David Wilson, Hydro Tasmania, 2004, personal commun.). Although not coinciding with a mapped fault, the Gell River scarp is close to, and parallels, the boundary between the Tyennan and Adamsfield-Jubilee strato-tectonic elements, as does the Lake Edgar scarp. The two scarps are separated by the Adamsfield ultramafic complex, which McCue et al. (2003) speculated acts to concentrate strain in the Lake Edgar–Gell River region.

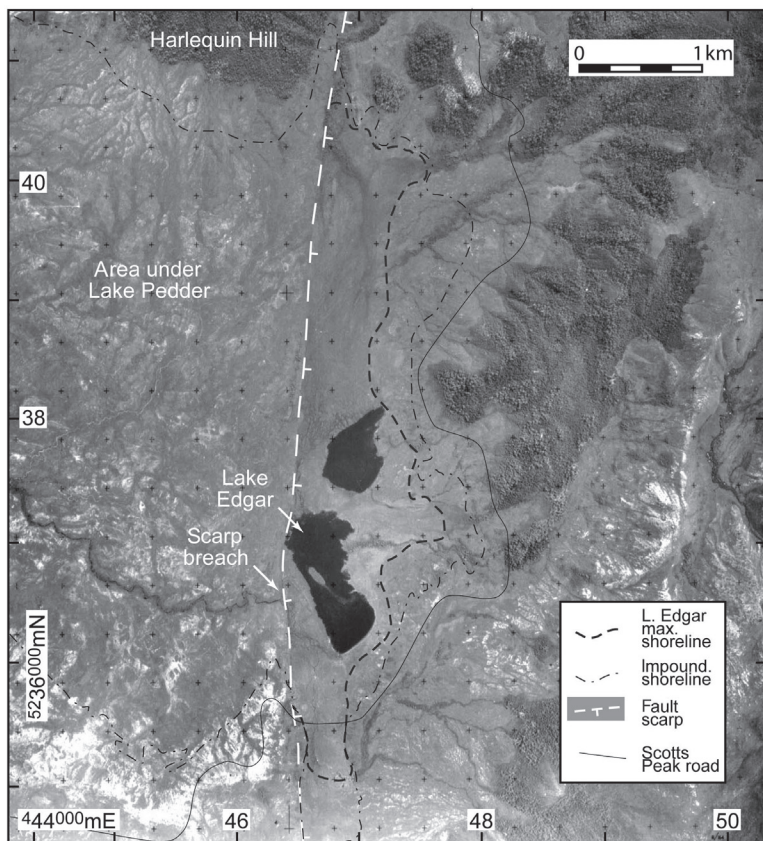


Figure 4. Former Lake Edgar and its companion lake (to the north) prior to flooding beneath the Lake Pedder reservoir. The inferred maximum level of Lake Edgar, which is bounded by the fault scarp on the west, and the current impoundment level are indicated. Note that a westerly flowing drainage breaches the scarp on the southwestern margin of Lake Edgar. Tick marks are shown on the downthrown side of the scarp. (Tasmania South West Project, Run 1, Image T360-23, 16 February 1961; image used with permission.)

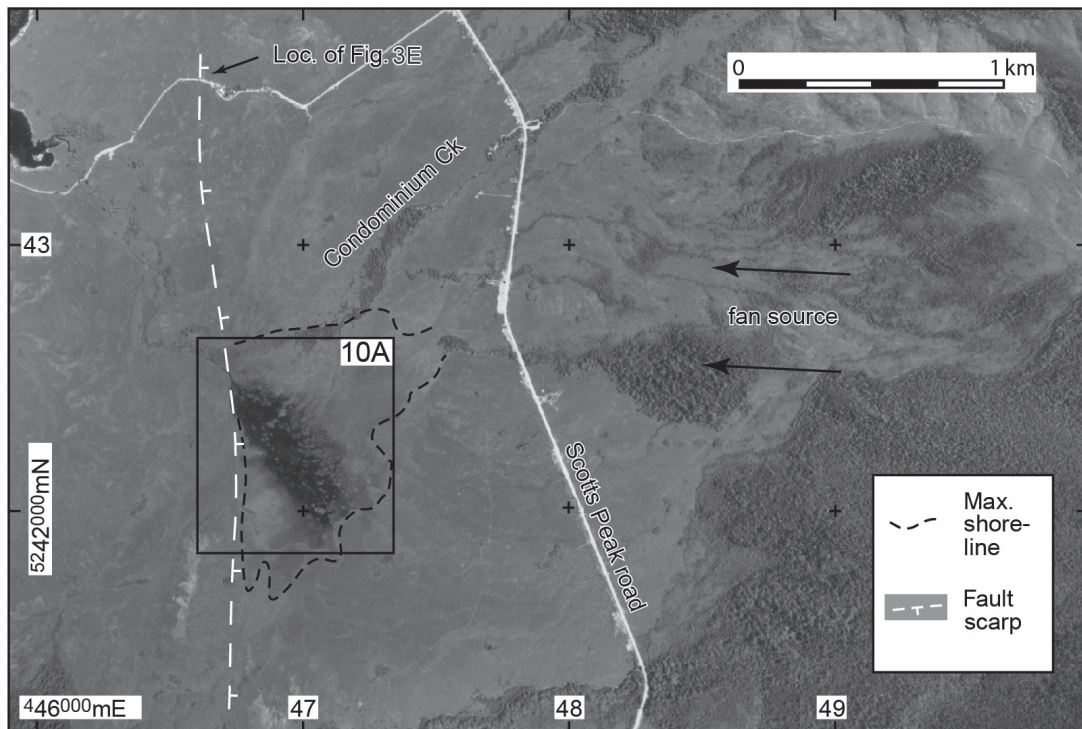


Figure 5. Aerial photograph of the sag pond to the north of Harlequin Hill, showing fan sources in the hills to the east. Location of Figure 10A is indicated. Tick marks are shown on the downthrown side of the scarp. (Tasmap 1:25,000, South West, Run 65, Image 008, 28 January 1988; image used with permission.)

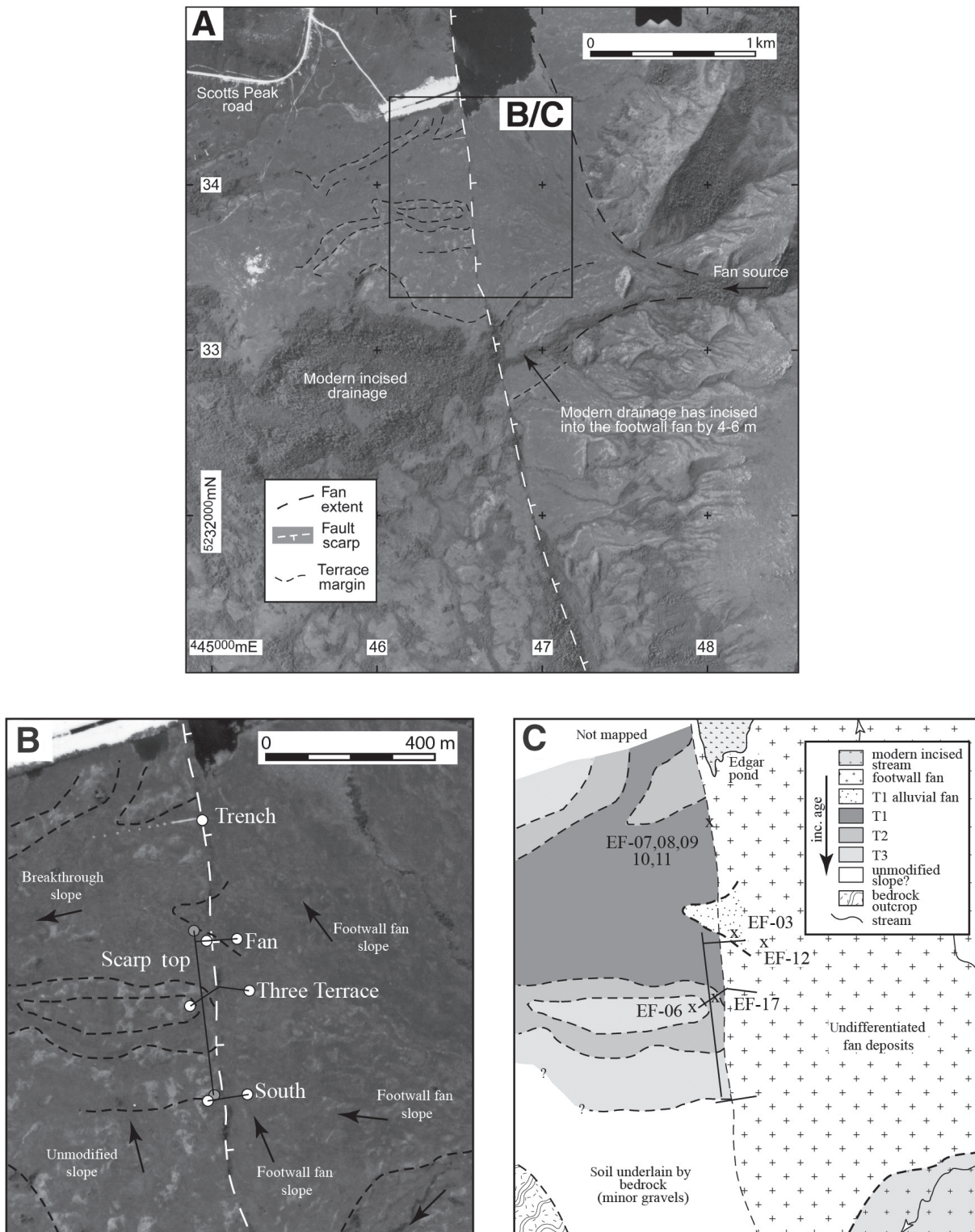


Figure 6. (A) Portion of aerial photograph showing study area location detail for profiles to the south of Edgar dam. The fan forming the source for the terraces investigated can be seen emanating from the hills to the east of the scarp. Locations of insets B and C are shown. (B) Detail of the geomorphology of the dissected fan showing location of profiles, transverse (scarp top) profile, and trench. White circles mark the ends of E-W profiles, and shaded circles mark the ends of the scarp top profile. Black arrows show the slope direction. (C) Map of geomorphic units (mainly terraces) identified in this study, with sample localities. Tick marks are shown on the downthrown side of the scarp. Flow directions on streams are shown by open arrow heads. (Tasmap, 1:25,000, South West, Run 68, Image 023, 28 January 1988; image used with permission.)

As is typically the case for stable continental region faults (e.g., McCue, 1990; Clark and McCue, 2003; Crone et al., 2003; Clark and Bodorkos, 2004), geomorphic evidence for Quaternary deformation in the Lake Edgar region is not complemented by a record of historic seismicity. Only two events of magnitude greater than three have been recorded in the region of Figure 1 (Shirley, 1980; Geoscience Australia online earthquake database, http://www.ga.gov.au/oracle/quake/quake_online.jsp, accessed November 2005). While both epicenters relating to these plot within 10 km of the Lake Edgar fault, the associated location uncertainties are large. For example, the larger event, of ~M 5.5, occurred in 1880 and was located using an isoseismal map (Michael-Leiba and Gaull, 1989). The position errors are likely to be of the order of 50 km or more.

Results: Scarp-Related Geomorphology

Although McCue et al. (2003) provided evidence for multiple Quaternary surface-rupturing events on the Lake Edgar fault, they did not obtain time constraints for the events. Here, we outline the geomorphic setting of samples for which we obtained chronological data relevant to the surface-rupture history of the Lake Edgar fault. We focused on two objectives for the study (Fig. 2): (1) dating the depositional ages of the sediments on the raised terraces south of Edgar dam (see McCue et al., 2003); and (2) dating the depositional history of sediment within a small sag pond located to the north of Harlequin Hill. These studies are described in detail subsequent to a discussion of the general scarp geomorphology.

General Scarp Geomorphology

The Lake Edgar fault scarp is clearly recognizable in aerial photographs (e.g., Figs. 4–6). Although it can be traced for almost 30 km (McCue et al., 2003), the southern half is the most pronounced. South of the Edgar dam abutment, the scarp is prominent on a periglacial fluvial fan that originates in the hills to the east (Fig. 3A). McCue et al. (2003) presented a model for the evolution of the geomorphology of this area that involved at least one surge of fan deposition having eroded the scarp before the fan was cut by subsequent faulting, thus forming a series of raised terraces on the hanging-wall block (Figs. 3B and 3C). These authors also suggested that till from the oldest glaciation in the area (ca. 2 Ma Eliza glaciation), which presumably underlies a higher terrace, is also cut by the fault. This area is discussed in more detail in the next section, in light of our recent work.

Aerial photography acquired in 1961 prior to the filling of the Lake Pedder impoundment (hereafter referred to as “Lake Pedder”) reveals that the former Lake Edgar and its smaller companion lake formed by ponding of westerly flowing streams against the upthrown western side of the fault scarp (Fig. 4). The texture of the land surface revealed in the aerial photography suggests that the lakes once formed part of a larger lake, which has either drained due to breaching of the scarp (a prominent breach

is labeled in Fig. 4) or drier climate, or it has been partially silted up (McCue et al., 2003). This area, totaling ~4 km of scarp length, is now submerged beneath Lake Pedder.

North of Harlequin Hill (Fig. 2), the scarp traverses a low-lying plain supporting a number of small streams originating on the Mount Anne/Mount Eliza massif to the east. The largest of these is Condominium Creek. Several of the streams enter a 600-m-long by 150-m-wide swampy pond, which drains through a 1.5–2-m-high breached scarp where the pond meets Condominium Creek (Figs. 2, 3D, and 5). The western boundary of the pond is defined by the fault scarp, suggesting that the pond owes its existence to reorganization of drainage following scarp formation, in a similar fashion to Lake Edgar. This pond is discussed in more detail in the section “Boring/Coring within the Fault-Bounded Pond.”

The hanging wall near the pond is modified by erosion. Adjacent to the pond, the scarp is sharp and well defined, rising 1.5–2 m above the pond surface level over a distance of less than 5 m. West of this initial rise, the land surface continues to rise in a staggered fashion before reaching a saddle ~5 m above the pond some 150 m west of its western margin. The land surface then drops off gently to the north, down to the shores of Lake Pedder. The lowest point in the saddle occurs where Condominium Creek has breached the scarp. This geomorphology suggests that a significant topographic barrier existed prior to the formation of the 2-m-high scarp that now bounds the pond. This barrier was largely removed by fluvial erosion focused along Condominium Creek prior to the formation of the most recent scarp.

The scarp becomes more prominent north of Condominium Creek, rising ~4.5–5 m over a horizontal distance of 10 m. The faulted scarp material is partly exposed along a track (see Fig. 5 for location), where it comprises an upper 200-mm-thick layer of peaty silt overlying sandy boulder gravel (Fig. 3E). Gravel clasts are as large as 150 mm in diameter and are highly weathered, some crumbling under hand pressure. The gravel lithology is mainly quartzite, with minor amounts of phyllite.

Further north, the scarp is lost within a cover of dense vegetation that bounds the Huon River. Aerial photography shows that the river course is remarkably straight for some 10 km north of this point, suggesting a continuation of the fault, if not the scarp.

Fluvial Terraces South of Edgar Dam

Three E-W-trending topographic profiles (profiles labeled Fan, Three terrace, and South in Fig. 6) were obtained south of Edgar dam to complement the three leveling profiles acquired by McCue et al. (2003). These were tied together with a profile along the top of the scarp. The location of the profiles with respect to the scarp and Scotts Peak Road is shown on Figure 6. A scarp-parallel profile across the footwall was not attempted. The morphology of the footwall was extrapolated from the three points on the E-W profiles where they reach the footwall fan.

The E-W profiles (Figs. 7B–7D) confirm the general westerly slope of the fan on both the hanging-wall and footwall blocks.

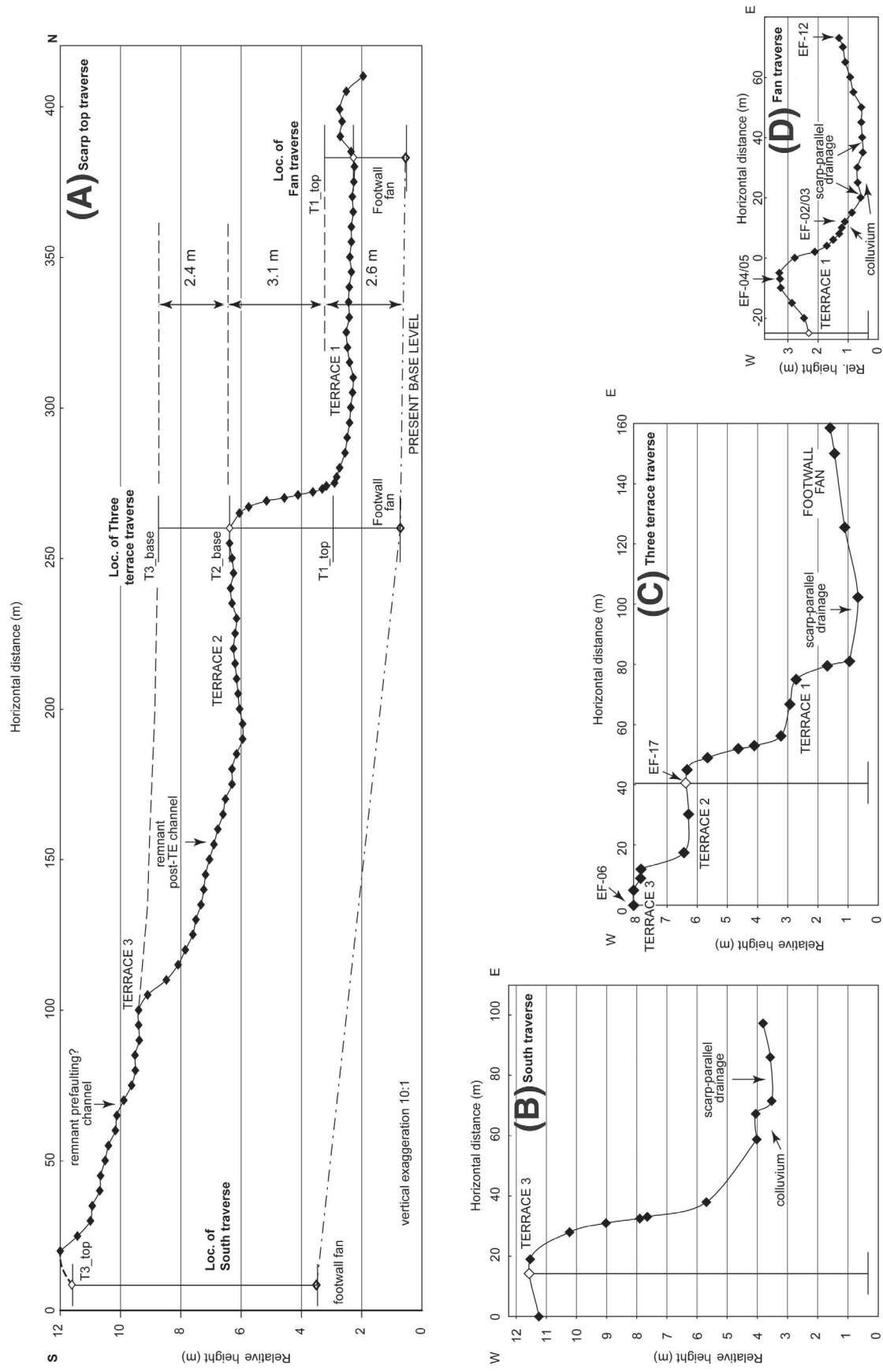
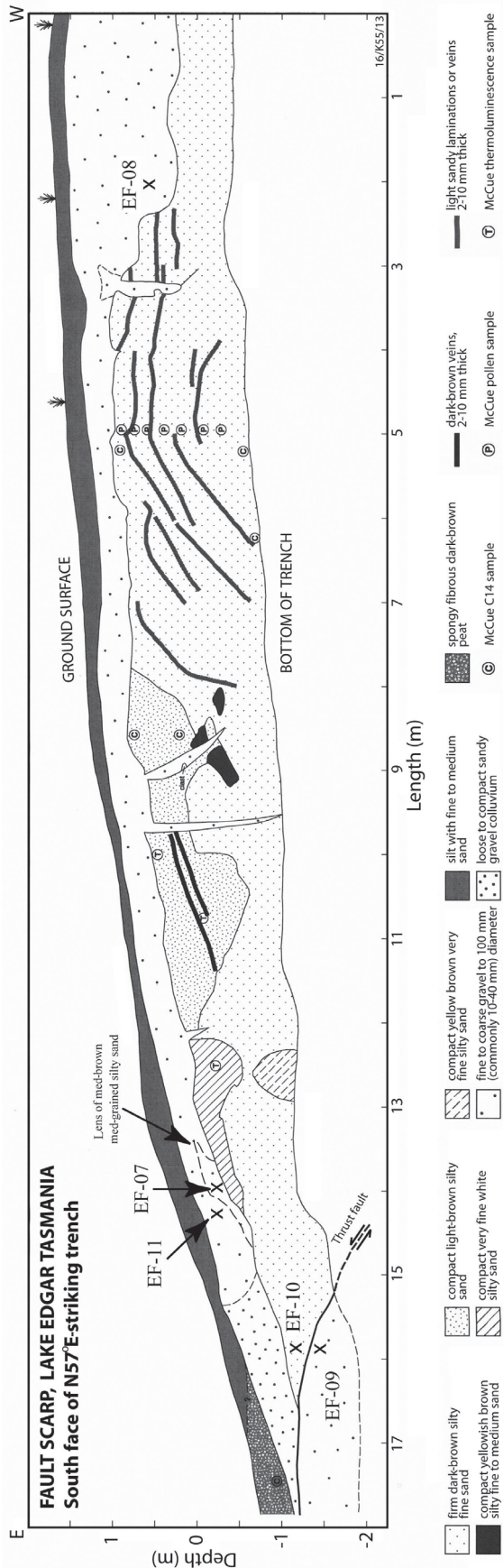


Figure 7. Leveling profiles over fluvial terraces on the upthrown western side of the Lake Edgar scarp. Locations of profiles are shown on Figure 6. (A) Scarp top traverse; (B) south traverse; (C) Three terrace traverse; (D) fan traverse.



The profiles also clearly show the two terraces on the hanging-wall block that were first identified by McCue et al. (2003). A third higher terrace is also clearly visible in the "Scarp top" traverse and the "Three terrace" traverse. South of the "Scarp top" traverse, the land surface on the up-thrown block continues to rise gradually. A shallow soil pit excavated ~200 m south of the profile encountered bedrock beneath a thin peaty veneer, and quartzite bedrock outcrops at the crest of the rise, some 500 m south of the profile. This indicates that the fan gravels give way to bedrock within a short distance south of the profile, and the scarp thereafter becomes bedrock controlled.

Shallow pits excavated on each terrace and on the footwall fan show an upper layer of peaty/sandy silt, 200–300 mm thick, overlying sandy fan gravels (Fig. 3F). The gravel clasts are 10 mm to over 150 mm in diameter, angular to subrounded, and predominantly quartzite. The gravel clasts on terraces 1 and 2 are fresh in appearance and significantly resistant to fracture when struck with a hammer, supporting the supposition of McCue et al. (2003) that they relate to glaciations younger than ca. 2 Ma. Gravel clasts on terrace 3 are significantly more weathered and can sometimes be crumbled in the hand, implying greater age, perhaps as old as the Eliza stage.

The trench excavation, which is situated on terrace 1 (McCue et al., 2003; Fig. 8), reveals that the gravels at this location form a sheet ranging from 0.5 to 1.0 m in thickness. This sheet is underlain by organic-rich silty sand. Our soil pits did not penetrate through the gravels on terraces 2 and 3, but it is plausible that they also form thin sheets mantling organic-rich silty sand and peat horizons.

The fan deposits on the footwall block rise in elevation toward the south, roughly mimicking the hanging-wall terracing. The stratigraphy of the footwall block does not show the distinct terracing observed in the hanging-wall block. However, we presume that an interbedded gravel and organic silty sand stratigraphy exists, similar to that on the hanging-wall block. A colluvial fan has developed at one location, redepositing material from terrace 1, and the scarp face, onto the footwall fan (see Fig. 7D; cf. Figs. 6B and 6C).

The terraced geomorphology described here is consistent with the evolutionary model of McCue et al. (2003), which involves erosional surges planing off the scarp before the fan was refaulted. However, our data suggest that three faulting events, not two, would have been required to produce the observed topography (Fig. 9). We found that the slot cut into the scarp following the penultimate faulting event is steep sided, whereas the profile of the fan prior to this was more U-shaped (Fig. 7). This might relate to the amount of time the fan had to establish a

Figure 8. Map of trench excavation in McCue et al.'s (2003) investigation. Sample locations for the McCue et al. (2003) study (thermoluminescence, pollen, and ^{14}C) and optically stimulated luminescence sample sites from this study are shown.

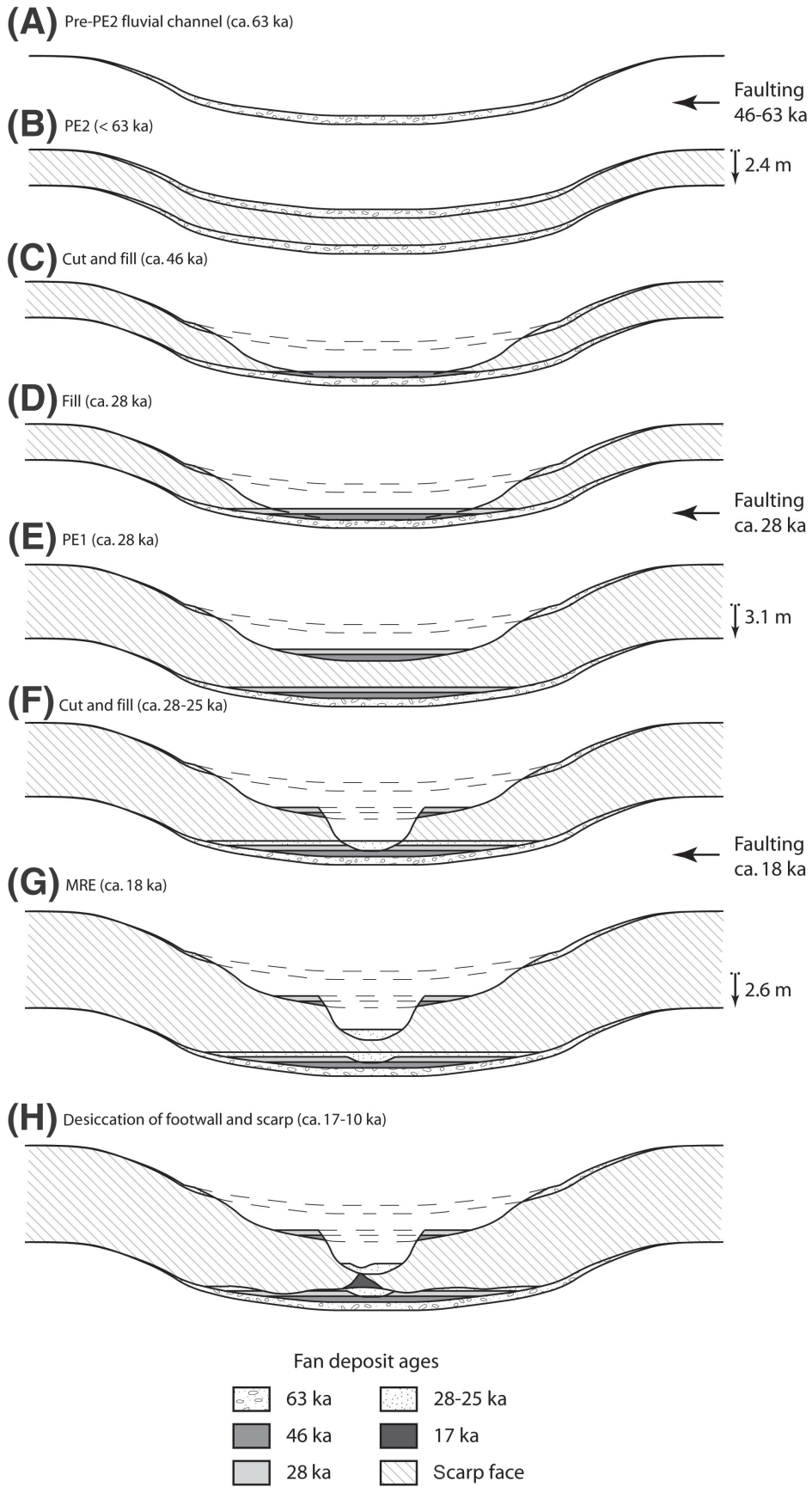


Figure 9. Schematic diagram depicting the history of events on the Lake Edgar fault, at the location shown in Figure 6A, as inferred from the terrace geomorphology (age ranges are discussed in the text). View direction is west. (A) Channel profile prior to the penultimate event 2 (PE2). (B) Channel profile displaced 2.4 m vertically across the fault by PE2. (C) Breaching and erosion of the PE2 scarp by a fan surge followed by gravel deposition. (D) Continuing fan activity resulting in additional gravel deposition. (E) Channel profile displaced 3.1 m vertically across the fault by the penultimate event 1 (PE1). (F) Breaching and erosion of the PE1 scarp by a fan surge followed by gravel deposition. (G) Channel profile displaced 2.4 m vertically across the fault by the MRE (most recent event). (H) Localized degradation of the composite scarp forming small alluvial/colluvial fans leading to the present-day configuration.

U-shaped equilibrium profile in each instance. An implication of this is that the time between breach of the penultimate event scarp and the cessation of fluvial activity was relatively brief.

Vertical displacement across the fault from each earthquake/faulting event can be estimated from the difference in elevation between the terrace surfaces (Fig. 7). The maximum difference in elevation between the level of the footwall fan and the top of terrace 1 (youngest) is ~2.6 m. This could be an underestimate of the true displacement during the most recent faulting event, because sediments may have accumulated at the base of the scarp following drainage defeat. The difference in height between the top of terrace 1 and the base of the U-shaped cut relating to terrace 2 (middle) is ~3.1 m, and the difference in elevation between the base of the terrace 2 cut and the base of the terrace 3 (oldest) cut (measured at the location of the “Three terrace” traverse) is 2.4 m.

The area investigated using scarp profiles during this study is located on the southern half of the scarp trace (cf. Figs. 2 and 6A). Because the along-fault displacement is generally characterized by displacement maxima near to the center of the trace (e.g., Hemphill and Weldon, 1999), it might be expected that the displacements measured here underestimate the maximum magnitude of displacement. The maximum slip is likely to have occurred in the region of the fault now submerged beneath Lake Pedder, perhaps 2.5 km south of Harlequin Hill. However, it is debatable whether the maximum relief would have been well preserved at this location prior to inundation, given that the Lake Edgar area was a focus for significant drainage concentration, and breaches of the scarp can clearly be seen in preflooding aerial photography (Fig. 4).

Boring/Coring within the Fault-Bounded Pond

A small pond situated east of Huon Inlet and north of Harlequin Hill, and bounded on its western side by the fault scarp, was also investigated in detail (Fig. 2). The lake relates to westerly flowing drainages that were impeded by faulting, most notably Condominium Creek.

The northwest corner of the pond has an outlet that breaches the scarp. Aerial photography suggests that the current lake area is about a third of the maximum attained previously (Fig. 5). Three core/boreholes were drilled within the lake using a combination of D-section and auger equipment to reveal the pond stratigraphy. The boreholes (Fig. 10) reveal a general stratigraphy consisting of an upper layer of dark-brown organic (peaty) mud overlying medium-grained white sand to clayey sand that becomes more clay-rich with depth. In turn, these sediments overlie dense clayey gravel, which is similar in character to the deposits on the uplifted fluvial terraces mentioned in the previous section. The clay matrix is interpreted as reflecting derivation of the sediments from the Mount Anne region, which is capped by dolerite, rather than from the quartzite ranges further south. The basal clayey gravel is therefore interpreted as prelake periglacial fluvial fan sediment. The auger would not penetrate the top of this horizon in hole numbers 2 and 3.

In the borehole closest to the scarp (hole 2), the basal dense clayey gravel is overlain by sandy clay and clayey/sandy gravel, which are interpreted as colluvium shed off the scarp. There is no evidence for cyclicity in the pond sediment that might indicate multiple cycles of faulting-induced sedimentation. This, together with the <3 m height of the fault scarp at this location, suggests that the present pond formed subsequent to the most recent faulting event.

OSL Geochronology

The study by McCue et al. (2003) included radiocarbon dating of samples from the trench locality on terrace 1 (e.g., Fig. 2). They dated samples from the peaty silt overlying the terrace 1 gravel sheet and also from silt underlying the gravel. The upper silt sample returned a modern age, whereas the lower silt samples gave ages older than 39,600 yr B.P., which exceeded the range of the radiocarbon technique. In light of this, and the geomorphic results presented here, we undertook an investigation using the

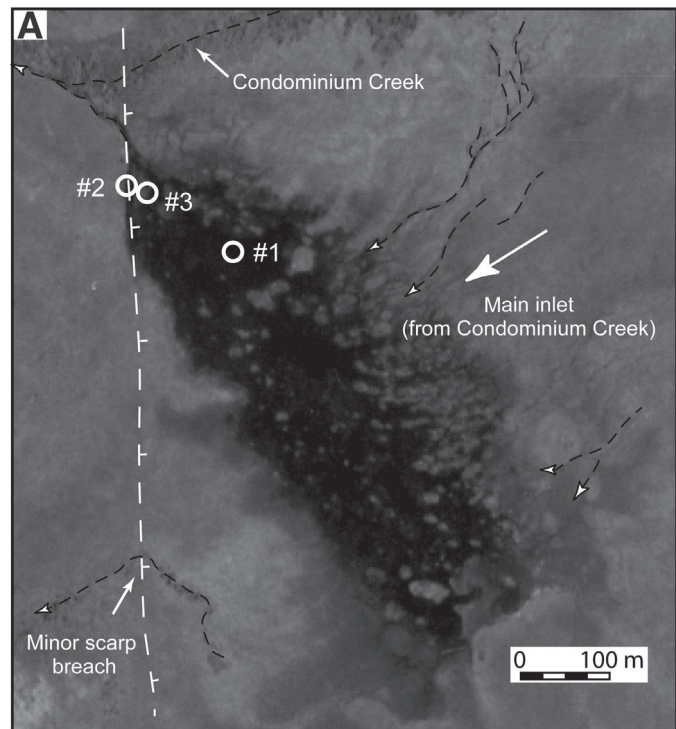


Figure 10 (*Continued on following page*). Detail of sag pond north of Harlequin Hill (location is shown on Fig. 5). (A) Borehole locations relative to the pond and scarp. Dashed lines represent streams. Flow directions on streams are shown by open arrow heads. (B) Stratigraphic sections revealed in boreholes. BWL—below water level; BOH—bottom of hole. For clarity, a schematic thickness of gravel has been added below the BOH in boreholes that terminated in gravel. Tick marks are shown on the downthrown side of the scarp.

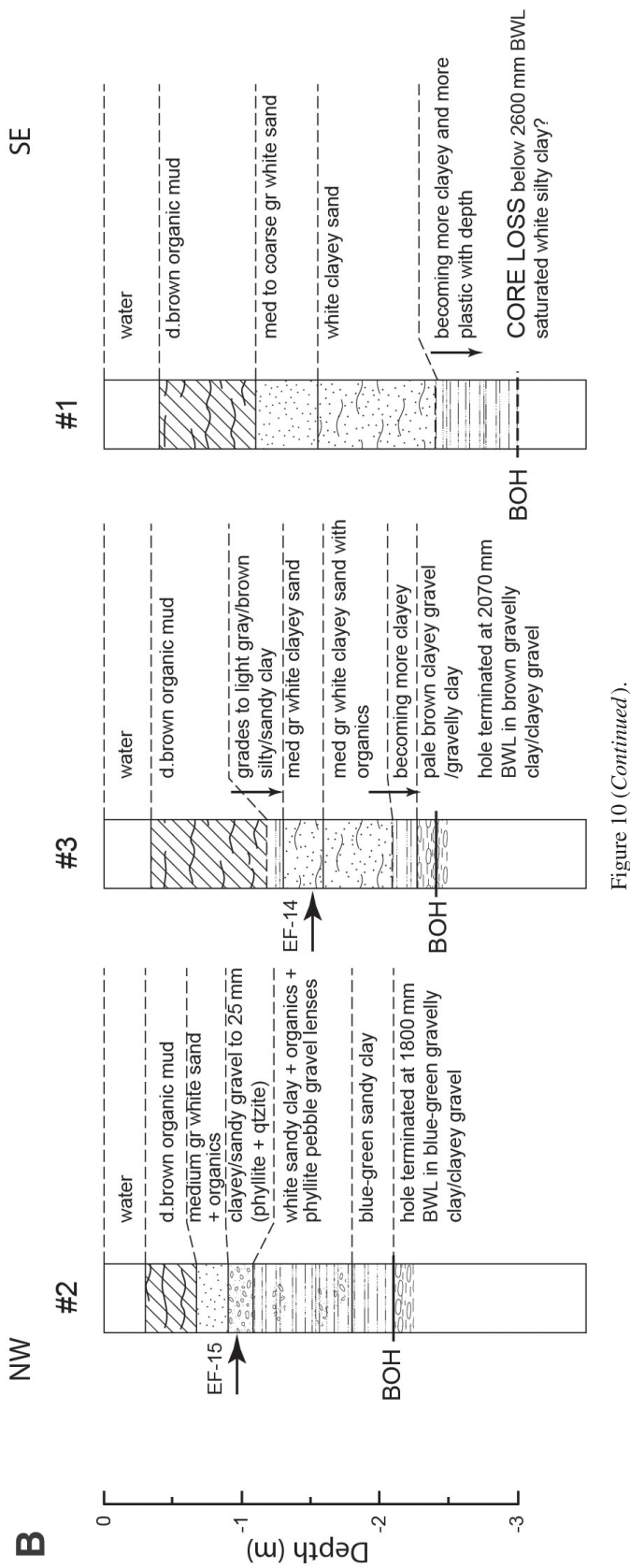


Figure 10 (Continued).

OSL technique to constrain faulting events by dating the gravelly sediments mantling the various terrace surfaces (see Appendix 1 for detailed sample context).

The single-aliquot regenerative dose (SAR) OSL protocol used in this study (see Appendix 2) measures the luminescence signals from multiple grain subsamples, each composed of ~100–200 quartz grains that are 90–125 µm in size. The limitation of multigrain dating is that heterogeneity that might exist in the sample, for example, due to incomplete resetting or bioturbation, is not completely resolvable. The degree to which quartz-rich sediment is reset during transport under various conditions and in different environments is beginning to be quantified using single-grain OSL (e.g., Olley et al., 2004). However, irrespective of problems with resetting, a multiple grain age determination on a sample will provide a maximum estimate for the depositional age of the sediment. In the context of the present study, age determinations on the sandy gravels deposited on the various terraces provide a maximum estimate for the time of faulting (i.e., uplift of the sediment above the level of deposition).

OSL Results and Age Constraints on Field Relationships

OSL dating of sandy gravel from near the surface of terrace 3 (EF-06, Appendix 1) produced a burial age of 61.3 ± 7.1 ka (Table 1; Fig. 11). This age provides an upper bound for the oldest recognized seismic event (the second penultimate event, PE2). An age of 28.0 ± 2.6 ka from a sandy gravel from terrace 2 (EF-17) provides a lower time bound for this event, and also an upper bound for the first penultimate event (PE1). Sandy gravels that mantle the lowest terrace (terrace 1) yielded burial ages of ca. 28 ka in the lower parts (EF-08, 28.8 ± 5.2 ka; EF-09, 28.1 ± 1.9 ka) and ca. 25 ka higher in the section, near the interface with the overlying peat (EF-11, 25.3 ± 4.0 ka). Although these ages are stratigraphically consistent, they are also statistically indistinguishable. They provide a lower bound for PE1 and an upper bound for the most recent event (MRE).

The MRE is constrained as having occurred subsequent to the 25.3 ± 4.0 ka deposition of sample EF-11 sandy gravels and prior to the 18 ± 0.8 ka deposition of gravelly alluvium/colluvium derived from terrace 1 (sample EF-03, 18.7 ± 1.3 ka; sample EF-15, 17.2 ± 1.0 ka).

The OSL results indicate that the sandy sediment underlying the mantle of gravel on terrace 1 (Fig. 8) is significantly older than the gravel itself. This confirms the reverse nature of faulting, showing that older sediment (EF-10) has been thrust over younger sediment (EF-09). Sample EF-07, obtained from a sandy lens at the base of the gravel, has a deposition age of 102 ± 14 ka. Dark-brown fine silty sand from EF-10, sampled from a stratigraphic level ~250 mm below the base of the gravel, was saturated with respect to OSL signal, and gave a minimum estimate of burial time of 173 ka. Sample EF-10 was taken from immediately above sample EF-09 (28.1 ± 1.9 ka), across the main MRE fault strand.

TABLE 1. OPTICALLY STIMULATED LUMINESCENCE (OSL) SAMPLE PROPERTIES AND AGE DATA (ERRORS ARE 1 σ)

Sample	Depth (m)	Water* (%)	Radionuclide concentrations [†]			α radiation [§] (Gy k.y. ⁻¹)	β radiation [#] (Gy k.y. ⁻¹)	γ radiation** (Gy k.y. ⁻¹)	Cosmic-ray radiation ^{††} (Gy k.y. ⁻¹)	Total dose rate ^{††} (Gy k.y. ⁻¹)	Equivalent dose ^{§§} (Gy)	OSL age (ka)
			K (%)	Th (ppm)	U (ppm)							
EF-03	0.3	15.0 ± 2.5	0.36 ± 0.01	2.13 ± 0.02	0.73 ± 0.02	0.03 ± 0.01	0.35 ± 0.02	0.19 ± 0.01	0.22 ± 0.02	0.79 ± 0.04	14.8 ± 0.8	18.7 ± 1.3
EF-06	0.4	12.5 ± 2.5	0.02 ± 0.01	1.00 ± 0.01	0.37 ± 0.02	0.03 ± 0.01	0.08 ± 0.02	0.03 ± 0.01	0.21 ± 0.02	0.36 ± 0.03	21.8 ± 1.9	61.3 ± 7.1
EF-07	0.7	20.0 ± 2.5	0.64 ± 0.01	3.04 ± 0.03	1.01 ± 0.01	0.03 ± 0.01	0.54 ± 0.02	0.16 ± 0.01	0.20 ± 0.02	0.93 ± 0.05	95 ± 13	102 ± 14
EF-08	1.4	15.0 ± 2.5	0.59 ± 0.01	1.62 ± 0.02	0.35 ± 0.03	0.03 ± 0.01	0.44 ± 0.02	0.22 ± 0.01	0.18 ± 0.02	0.87 ± 0.04	25.0 ± 4.4	28.8 ± 5.2
EF-09	1.1	15.0 ± 2.5	0.75 ± 0.01	2.48 ± 0.02	0.91 ± 0.01	0.03 ± 0.01	0.62 ± 0.03	0.25 ± 0.02	0.20 ± 0.02	1.10 ± 0.05	30.9 ± 1.6	28.1 ± 1.9
EF-10	0.9	30.0 ± 5.0	1.75 ± 0.02	7.33 ± 0.06	2.15 ± 0.02	0.03 ± 0.01	1.27 ± 0.07	0.23 ± 0.02	0.20 ± 0.02	1.73 ± 0.11	>300	>173
EF-11	0.5	15.0 ± 2.5	0.50 ± 0.01	1.41 ± 0.02	0.33 ± 0.03	0.03 ± 0.01	0.37 ± 0.02	0.07 ± 0.01	0.21 ± 0.02	0.69 ± 0.04	17.4 ± 2.5	25.3 ± 4.0
EF-12	0.4	15.0 ± 2.5	0.47 ± 0.01	1.56 ± 0.02	0.54 ± 0.02	0.03 ± 0.01	0.38 ± 0.02	0.16 ± 0.01	0.21 ± 0.02	0.79 ± 0.04	37.7 ± 5.6	47.7 ± 7.5
EF-14	1.3	40.0 ± 5.0	1.23 ± 0.01	7.31 ± 0.06	2.34 ± 0.02	0.03 ± 0.01	0.93 ± 0.05	0.63 ± 0.02	0.18 ± 0.02	1.77 ± 0.08	19.5 ± 0.9	11.0 ± 0.7
EF-15	0.8	40.0 ± 5.0	1.24 ± 0.01	7.13 ± 0.06	1.63 ± 0.02	0.03 ± 0.01	0.87 ± 0.05	0.57 ± 0.02	0.20 ± 0.02	1.66 ± 0.08	28.6 ± 1.1	17.2 ± 1.0
EF-17	0.3	12.5 ± 2.5	0.02 ± 0.01	1.26 ± 0.02	0.68 ± 0.02	0.03 ± 0.01	0.12 ± 0.01	0.22 ± 0.02	0.49 ± 0.03	13.8 ± 1.0	28.0 ± 2.6	

*Estimated time-averaged moisture contents, based on measured field water values (% dry weight).

[†]Obtained by instrumental neutron activation analysis (INAA; Becquerel Laboratories, Menai).[§]Assumed internal alpha dose rate.[#]Derived from INAA radionuclide concentration measurements, corrected for attenuation by water and beta attenuation.^{**}Derived from field gamma spectrometry for EF-03-EF-12; INAA radionuclide concentration measurements for EF-14-EF-17, corrected for attenuation by water.^{††}Calculated using the equation of Prescott and Hutton (1994), based on sediment density, time-averaged depth and site latitude, longitude and altitude.^{§§}Including a ±2% systematic uncertainty associated with calibration of the laboratory beta source.

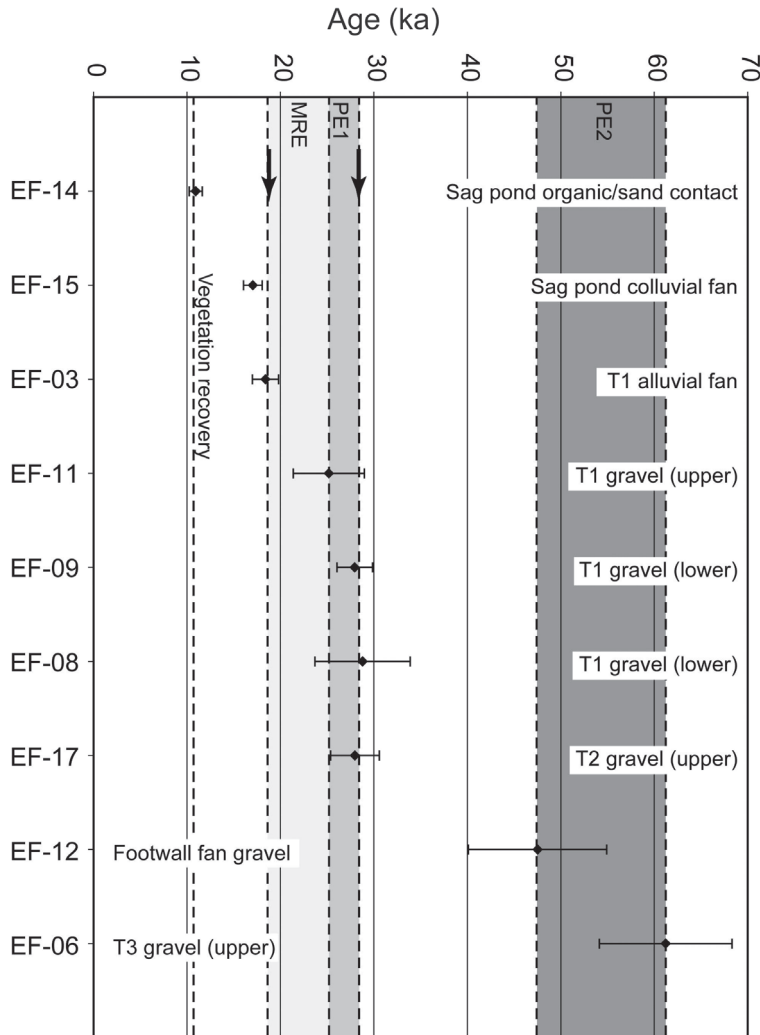


Figure 11. Ages from the optically stimulated luminescence samples with 1σ error bounds. Constraints on the timing of the three events are provided by the samples as shown. EF-10, at older than 173 ka, occurs off the top of timescale. Black arrows show the preferred ages of MRE and PE1. MRE—most recent event, PE1—first penultimate event, PE2—oldest recognized event.

The 11.0 ± 0.7 ka age obtained from sample EF-14 provides a maximum estimate for the timing of the change from clastic- to organic-dominated sedimentation in the fault-bounded lake. Deposition within the lake did not involve a discernible organic component at the time of colluvial sediment accumulation (i.e., immediately after the MRE); in fact, there is no evidence of significant organic material accumulation until after 11 ka.

DISCUSSION

Timing and Magnitude of Paleo-Earthquakes on the Lake Edgar Fault

Most Recent Event

The timing of the most recent faulting event (MRE) is bracketed by the ages obtained on the faulted terrace 1 gravels (EF-11, ca. 25 ka) and by the ca. 17–19 ka ages derived from the unfaulted colluvium derived from the uplifted deposits of terrace

1 (the average age of samples EF-03 and EF-15 is 18 ± 0.8 ka). This range, ca. 18–25 ka, spans the time of the LGM in the Australasian region, when average temperatures were ~ 9 – 10 °C lower than today (Miller et al., 1997; Barrows et al., 2001). The dominance of clean clastic sediment poor in organic peat content suggests that this was also a time of great aridity in the Lake Edgar region, with little or no vegetative cover on the valley floors. This interpretation is supported by the extent of colluvial deposits that were shed from the MRE scarp, despite the low angle of the MRE fault trace (Fig. 8), which is unlikely to have formed a free face subsequent to rupture. The accumulation of colluvium following the MRE may have been rapid compared to a fully vegetated region. Hence, we propose that the MRE faulting occurred immediately prior to the deposition of the colluvium shed off terrace 1 at ca. 17–19 ka (Fig. 11).

McCue et al. (2003) argued that the MRE occurred in the very recent past based upon the prominence of the scarp, despite a current, relatively high average annual rainfall. Although our

age data are incompatible with this interpretation, some explanation of the apparent youth of the landform is warranted. At present, there is almost no erosion and transport of clastic sediment because the landscape has been completely stabilized by vegetation (button grass plains, swamps, etc.). The geomorphological evidence suggests that the landscape has been in a stable form for the entire Holocene, and perhaps longer (Kiernan, 2001). The transition from clastic deposition (e.g., landscape instability and erosion) to organic deposition (landscape stabilized) probably occurred between 10 ka and 13 ka (this study; Michael Fletcher, 2003, personal commun.). Hence, there may have been a window of as little as 3 k.y. (to as much as 10 k.y.) between scarp formation and stabilization of the landscape. In this interval, it is likely that there was some vegetation acting to retard erosion. This, in combination with the low angle of the fault trace where it approaches the surface (we speculate that there was never a free face), is proposed to account for the preservation in the landscape of the youthful appearance of the scarp.

It is difficult to estimate the magnitude of the earthquake that formed the 2.6-m-high MRE scarp with certainty since the length of the surface rupture is not well constrained, nor is fault dip known at seismogenic depth. The air photograph lineaments associated with significant Quaternary expression of faulting extend for ~20 km. However, a significant linear topographic break, which coincides with the inferred position of the Lake Edgar fault, and which controls the path of the Huon River, extends for another 10 km to the north of the scarp (Fig. 2). The empirical relationships among scarp height, fault length, and earthquake magnitude developed by Wells and Coppersmith (1994) suggest that the height of the MRE scarp relates to an earthquake of M_w 6.8 ± 0.5 , assuming that the fault dips steeply 65° – 70° to the west at depth, and that slip is predominantly downdip. Such a magnitude is consistent with a scarp length of 25–30 km. If the dip of the Quaternary fault at depth is more shallow than the near-surface drilling results suggest (Roberts et al., 1975), then a larger event would be required to generate the observed relief (because the downdip width of the fault would be considerably more). As mentioned in a previous section, the location of our scarp profiles on the southern portion of the fault trace also raises the possibility that the vertical relief figures calculated for each event underestimate the maximum values obtained. This would also lead to an underestimate of the magnitude.

Penultimate Event 1

The near coincidence of ages from surfaces of terrace 1 (EF-08 and -09) and terrace 2 (EF-17) is consistent with the penultimate faulting event having occurred during active fluvial/alluvial deposition ca. 28 ka (the average of the ages of EF-08, EF-09, and EF-17 is 28.3 ± 2.0 ka). This interpretation is consistent with unpublished data suggesting widespread landscape instability and eolian deposition in the lower Huon River at this time (P. McIntosh and K. Kiernan, 2004, personal commun.). An alternative is that fluvial deposition had ceased prior to PE1 faulting, and that footwall fan gravels and sands of ca. 28 ka age were

transported at a later date onto the hanging wall without resetting their OSL systematics, but this hypothesis seems unlikely. However, the 47.7 ± 7.5 ka age obtained on sandy gravel sampled on the footwall fan adjacent to the midsection of the terrace 1 deposits (sample EF-12) indicates that sediments with a range of depositional ages are preserved on the footwall fan, and may have provided mixed age sources for the terrace gravels. Nonetheless, the ca. 28 ka age obtained on sample EF-17 from the top of terrace 2 provides a maximum time bound for PE1 (Fig. 11).

There appears to be ~3.1 m of change in base level of the fluvial fan as a result of the first penultimate event. This single-event vertical displacement is slightly larger than that resulting from the MRE (2.6-m-high scarp), and it may have been generated by an event of M_w 6.9 ± 0.6 (well within error of the estimate for the MRE). The relationships of Wells and Coppersmith (1994) suggest that this event may have ruptured the entire 45 km length of the Lake Edgar fault.

Penultimate Event 2

The time of the second penultimate event, PE2, is broadly bracketed by the ca. 61 ka (61.3 ± 7.1 ka) age obtained on terrace 3 gravel and the ca. 28 ka (the average of samples EF-08, EF-09, and EF-17 is 28.3 ± 2.0 ka) age obtained on terrace 2 gravel. Further constraint is provided by the 48 ka (47.7 ± 7.5 ka) age obtained on a sample of the footwall fan gravel. Although terrace 3 has not been thoroughly sampled, the location of sample EF-06 near the center of the depositional channel that breached the scarp makes it highly likely that ca. 48 ka gravel would have been preserved had they existed. It is reasonable to assume that the ca. 48 ka gravel identified in the footwall reflects a phase of fluvial activity similar to those that resulted in the deposition of the ca. 61 ka and ca. 28 ka gravels, as this time coincides with a period (of probable landscape instability) between glacial advances identified in New Zealand (Williams, 1996; Barrows et al., 2002; Fink and Williams, 2003) and the Kosciuszko region of Australia (Barrows et al., 2001). The absence of gravel of this age on terrace 3 thus implies that PE2 predated ca. 48 ka. We therefore propose that the PE2 occurred between 48 ka and 61 ka (47.7 ± 7.5 ka to 61.3 ± 7.1 ka) (Fig. 11).

The relief relating to PE2 is similar to that generated in the younger two events. A causative earthquake of a similar magnitude is implied.

Older Quaternary Fault Activity

There is no evidence in the trench, nor conclusive evidence in the geomorphology, for surface-rupturing earthquakes prior to PE2. Although the continued rise of the upthrown block to the south of the “Scarp top” traverse may relate to pre-PE2 seismic activity, we found no markers that might conclusively demonstrate this. Two explanations for the apparent lack of pre-PE2 events are plausible: (1) There were no Quaternary events prior to the PE2; or (2) any geomorphic expression relating to previous events has been planed off by ice, destroyed by other erosive processes, or buried by sediment accumulation.

Implications of the Data for Seismic Hazard Assessment

The Lake Edgar fault is undoubtedly susceptible to reactivation under conditions imposed by the modern Australian intraplate stress field. The history of recurrence of large surface-rupturing earthquakes established herein, with the last (MRE) event having occurred in the past 20 k.y., requires that the Lake Edgar fault be classed as an active (or capable) fault (e.g., IAEA, 1991; USNRC, 1996; Machette, 2000). The data presented herein also provide fundamental insight into the behavior of intracratonic faults and have associated implications for hazard assessment, as discussed next.

Fault Behavior

The results of the geochronology and geomorphic analysis indicate surface-rupturing earthquakes on the Lake Edgar fault at around 17–19 ka (18.0 ± 0.8 ka), 26–30 ka (28.3 ± 2.0 ka), and 40–68 ka (47.7 ± 7.5 – 61.3 ± 7.1 ka). The interseismic intervals are thus 7–13 k.y. and 10–42 k.y., with ~18 k.y. having elapsed since the last surface rupture. While this close temporal clustering of large earthquakes is remarkable for an Australian stable continental region fault, it is possible that the last three events on the Lake Edgar fault are atypical of the long-term behavior of the fault. Investigations of stable continental region faults elsewhere in Australia and in the eastern United States (Crone and Luza, 1990; Crone et al., 1992, 1997, 2003) found earthquake recurrence behavior to be characterized by relatively short-lived periods of activity separated by long periods of quiescence. The inter-event times between successive earthquakes in the short-lived active periods can range from hours (e.g., the 1988 Tenant Creek earthquake sequence; Crone et al., 1992) to thousands of years (e.g., the Meers and Cheraw faults; Crone and Luza, 1990) to tens of thousands of years (e.g., the Hyden and Roopena faults; Crone et al., 2003). The periods of quiescence can be as long as millions of years or more (e.g., the Hyden fault; Crone et al., 2003).

It is noteworthy that the three events identified on the Lake Edgar fault have resulted in the generation of similar amounts of vertical relief. The concept of a “characteristic event” (Schwartz and Coppersmith, 1984) might therefore be applicable to this fault (i.e., surface-breaking earthquakes are of similar magnitude). There is no evidence in the geomorphology, nor in the trench profile, indicative of smaller events between the three major surface ruptures. In addition, our OSL data effectively rule out the possibility of fault creep (or a series of small events) having formed the observed relief, as opposed to three large discrete events. If this were the case, the deposits on terrace 1 and terrace 2 would be of significantly different ages (at least 13 k.y. difference, assuming the upper bound slip rate of 0.24 mm/yr; see next section) rather than of similar age (i.e., ca. 28 ka).

Slip Rate

Providing an estimate of the slip rate in which we might have confidence is difficult for intraplate faults, where the recurrence

for surface-rupturing events is measured in thousands to many tens of thousands of years. Not only do interseismic intervals far exceed the record of historical seismicity, there is also the possibility that displaced geomorphic datums might be significantly altered by erosion. The problem is compounded if earthquakes exhibit temporal clustering, as may be the case for the Lake Edgar fault, because slip rates should then be averaged over a time period containing a large number of seismic cycles.

Information from two complete seismic cycles on the Lake Edgar fault is preserved within the area of investigation. Given that the scarp remains a sharp feature in the landscape, it is not expected that erosion of the scarp (other than by localized fluvial activity) has significantly reduced the scarp height, subsequent to the last three events at least. Figure 12 presents a graphical summary of the timing of displacement events. The slip rate for the seismic cycle PE1–MRE is 0.25 ± 0.05 mm/yr, whereas that for the cycle PE2–PE1 is between 0.09 ± 0.02 and 0.16 ± 0.07 mm/yr. Estimates for the average slip rate calculated over the two complete seismic cycles range between 0.13 ± 0.02 mm/yr and 0.19 ± 0.05 mm/yr (i.e., a total range including uncertainties of 0.11 – 0.24 mm/yr).

The average slip rate on the Lake Edgar fault appears large compared to those inferred for other intracratonic faults in Australia, even where significant fault-controlled relief is evident. For example, faults bounding the Mount Lofty and Flinders Ranges in South Australia, which are responsible for the generation of significant Quaternary relief (several tens of meters), have average slip rates estimated at 0.02–0.03 mm/yr for the past 3–5 m.y. (Sandiford, 2003a). The same author reported similarly low slip rates of 0.01–0.02 mm/yr from faults in the central Murray Basin and rates of as much as 0.1 mm/yr from the Otway Ranges in Victoria, all averaged over a similar time period (Sandiford, 2003a, 2003b). These lower slip rates are perhaps more consistent with the low strain accumulation rates that might be expected from a stable continental region, which might in general be considered incapable of sustaining long sequences of closely temporally clustered (e.g., recurrence intervals of thousands of years) large earthquakes. Intuitively, each successive earthquake in a temporally clustered sequence on a stable continental region fault might be expected to dramatically decrease the likelihood of a near-future recurrence.

It is not possible to tell if the slip rate calculated from the last two complete seismic cycles on the Lake Edgar fault is representative of the long-term (i.e., hundreds of thousands to millions of years) slip rate on the fault because there is no evidence for events prior to PE2. While this discussion suggests that the last two seismic cycles may not be representative of the longer term, the possibility that the Lake Edgar region is anomalous in terms of strain accumulation rate must also be considered. As mentioned in the section on “Regional Geomorphology and Evidence for Quaternary Deformation,” it is plausible that strain is concentrated in the Lake Edgar and Gell River areas as a consequence of the rheology contrasts between the Adamsfield ultramafic complex and adjacent rocks abutting the contact between

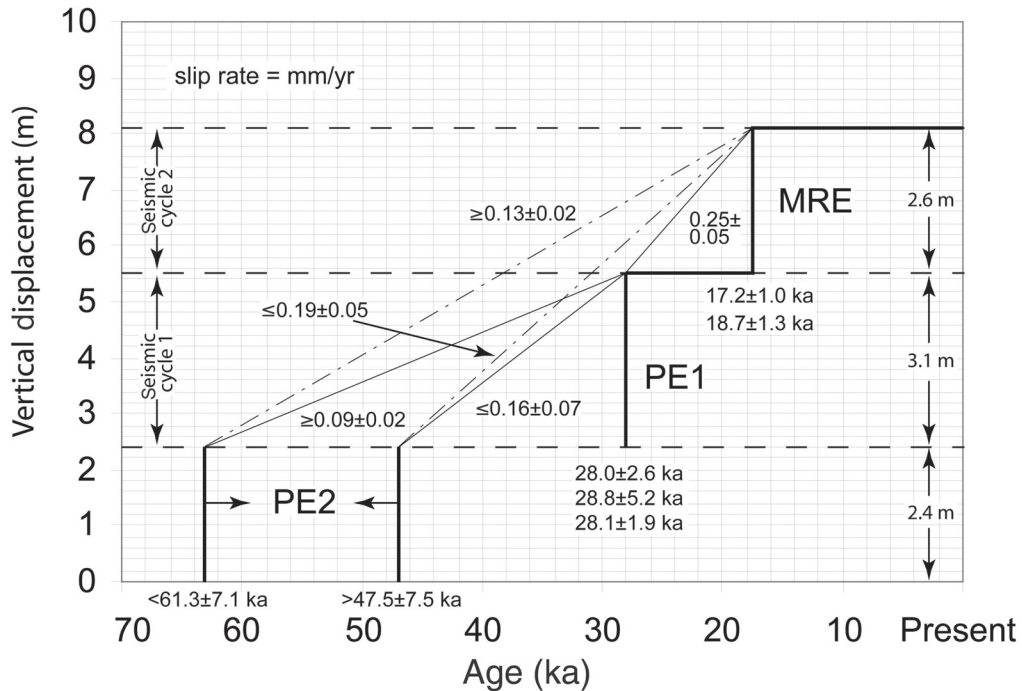


Figure 12. Slip rate estimates for the late Quaternary activity on the Lake Edgar fault. Uncertainties in ages are 1 standard deviation. Where several age determinations constrain the timing of an event (e.g., three samples date the first penultimate event [PE1]), the average of those measurements (with appropriate error propagation) was used for slip rate calculation. MRE—most recent event, PE2—oldest recognized event.

the Tyennan and Adamsfield-Jubilee tectonic elements (McCue et al., 2003; Fig. 1).

Implications for Climate and Glaciation in SW Tasmania

Cosmogenic-nuclide dating of the Timk and Judd moraines on Schnells Ridge (6 km east of the Lake Edgar fault) yielded ages of ca. 19 ka for the maximum extent of the most recent glaciation (LGM) that has affected the area (Kiernan et al., 2004). Dating elsewhere in Tasmania suggests that the late LGM occurred at around 20 ka, with retreat by 18 ka (Colhoun and Fitzsimons, 1990; Barrows et al., 2002; Colhoun, 2003). No firm age control exists on glacial deposits in the Lake Edgar region that predate the LGM. However, Kiernan et al. (2004) reported cosmogenic nuclide exposure ages of ca. 40 ka and ca. 70 ka for individual boulders from the composite Timk moraine, which correspond to periods of glaciation identified from moraines in southeastern Australia (39–46 ka and >59 ka; Barrows et al., 2001) and from southern New Zealand (41–45 ka and 65–75 ka; Williams, 1996; Fink and Williams, 2003). Glacial advances have also been documented in the South Island of New Zealand between 25 and 28 ka, at 19–21 ka, and at 14–17 ka (Fink and Williams, 2003). Given the correspondence between Timk and Judd moraine ages and the timing of glacial events in New Zealand, and the likely-

hood that the New Zealand cold climate episodes reflect regional rather than local climatic influences, it might also be expected that cold climate episodes occurred in Tasmania between 28 and 25 ka and at 17–14 ka.

The ages obtained from the fan gravels along the Lake Edgar fault suggest episodes of landscape instability at ca. 61, ca. 48, ca. 28–25, and ca. 17–11 ka. Considering the dating errors, these ages correspond well to cold climate episodes recognized in southeastern Australia and New Zealand. Therefore, we propose that the landscape instability, which leads to the deposition of sediments in fans in the Lake Edgar region, resulted from a reduction of vegetative cover as a consequence of cold climate. A probable climatic trigger for fan formation is best demonstrated by age of the youngest fans (ca. 17–19 ka), which formed immediately after the initiation of retreat from the LGM. The deposition of colluvial deposits in fans over the low-angle surface rupture following the most recent faulting event (ca. 17–19 ka) implies that vegetation did not effectively stabilize the landscape at this time. We believe that the age of 11.0 ± 0.7 ka (EF-14) obtained immediately below the sand-organics interface in the fault-bounded pond to the north of Harlequin Hill provides important time constraints on the recovery of vegetation after the end of the last glaciation. Hence, if precipitation had returned to values similar to today prior to the reestablishment of vegetation, then some

potential may have existed for slope instability, fan formation, and the shedding of sandy sediment into lakes. In a lacustrine setting, it might be expected that once vegetation restabilized the landscape, this influx of sandy sediment would be much reduced, and potentially be overwhelmed by organic sediment, producing the sediment profile revealed in the boreholes.

The temporal relationship between the older periods of fan activity (pre-LGM) and cold climate episodes is not clear at the resolution of our age data. The reestablishment of relatively high postglacial rainfall levels prior to vegetation recovery provides a plausible mechanism for fan reactivation, as described previously. However, the older fans were far more extensive and energetic than the youngest fans and resulted in major localized erosion of the Lake Edgar fault scarp. We speculate that this reflects a higher annual rainfall budget than today, or more meltwater contribution to the Huon River catchment than today.

CONCLUSIONS

The main findings of this study are as follows: (1) Three recognizable surface-rupturing earthquakes have occurred on the Lake Edgar fault in the past 48–61 k.y., with the most recent event (MRE) occurring some 17–19 k.y. ago; (2) each event on the ~45-km-long fault is associated with ~2.4–3.1 m of vertical displacement at our study site, implying a *characteristic* moment magnitude event in the order of Mw 6.8–7.0, which is comparable to the largest earthquake events recorded in Australia; (3) the average slip rate calculated for two complete earthquake cycles ranges from 0.11 to 0.24 mm/yr, which is large compared to other stable continental region faults; and (4) the timing of latest Pleistocene fluvial fan deposition suggests previously unrecognized cold climate episodes in SW Tasmania at ca. 61 ka, ca. 48 ka, and ca. 28–25 ka.

ACKNOWLEDGMENTS

Mike Machette and Buddy Schweig are thanked for their constructive reviews of the manuscript. We thank Hydro Tasmania

for allowing us access to their lands and for comments relating to the original manuscript. We appreciate permission from the Tasmanian Department of Primary Industries, Water and Environment to conduct research in the Southwest National Park, and for field assistance. Matt Hayne of Geoscience Australia also provided valuable field assistance, and provided useful comment on the original manuscript. This work is published with the permission of the Chief Executive Officer of Geoscience Australia.

APPENDIX 1. CONTEXT OF THE DATED SAMPLES

Sand and sandy gravel from five localities within the trench (Fig. 8), two locations within the sag pond (Figs. 10A and 10B), and four locations on various fluvial terraces (Figs. 6C and 7) were collected for single-aliquot regenerative-dose (SAR) OSL dating of quartz grains. The results of the analyses are presented in Table 1. Analytic procedures are presented in Appendix 2. The following abbreviations are used: HB—hanging-wall block; FB—footwall block. Global positioning system coordinates are provided in the WGS84 datum using a UTM projection (zone 55S) (Table A1).

Upper Part of Gravel Mantle at Trench Locality, HB (Sample EF-11) 55G, 446654 mE, 5234465 mN

Sample EF-11 is from the south face of the trench excavation (Fig. 8). An account of the detailed trench stratigraphy is published in McCue et al. (2003) and is not reproduced here. However, the general stratigraphy consists of a 200–300-mm-thick layer of peaty silt with fine to medium sand, which mantles the ground surface and overlies a 500–1100-mm-thick layer of fine to coarse gravel (clasts typically 10–40 mm, but up to 100 mm). The sampled gravel is poorly sorted and contains angular and subrounded clasts predominantly of quartzite and vein quartz. Clasts typically appear reasonably fresh and will ring if struck with a hammer. A soil pit excavated into terrace 1 next to

TABLE A1. COORDINATES OF LOCATIONS IMPORTANT TO THIS STUDY

Feature	Easting (mE)	Northing (mN)	Elevation (approx. m)
Lake Edgar	446900	5236400	<302
Companion lake to Lake Edgar	447100	5237200	<302
Sag pond north of Harlequin Hill	468600	5242300	314
Fan traverse (west end)	446665	5234179	317
Three terrace traverse (west end)	446629	5234025	332
South traverse (west end)	446667	5233800	321
Scarp top traverse (center)	446648	5234046	316
Trench	446654	5234465	310
Borehole 1	446957	5242553	314
Borehole 2	446836	5242629	314
Borehole 3	446858	5242621	314
Gell River scarp	437000	5302000	560

Note: Coordinates are based on WGS 84 datum and UTM projection, zone 55S.

the trench confirmed the competency of the gravel clasts, and that the upper surface of the gravel is the terrace 1 surface. The gravel layer overlies firm dark-brown silty fine sand that extends to the base of the trench.

OSL sample EF-11 was taken near the top of the gravel sheet mantling the scarp on the hanging-wall block. The age of the sample provides a maximum time bound for the most recent faulting event, since the gravel mantle is cut by the most recent event (MRE) on the fault.

**Lower Part of Gravel Mantle at Trench Locality, HB
(Sample EF-08)**

55G, 446654 mE, 5234465 mN

Sample EF-08 is from the south face of the trench excavation (Fig. 8), within the lower half of the gravel that mantles the scarp on the hanging-wall block. The gravel unit thickens markedly at the sampling site compared to elsewhere in the trench. Stratigraphy within the underlying sediment is truncated upward at the gravel interface, suggesting that the irregular gravel thickness is in a channel. The sample was taken to provide an indication of the age structure of the gravel that is displaced by the most recent faulting event (MRE).

**Lower Part of Gravel Mantle at Trench Locality, FB
(Sample EF-09)**

55G, 446654 mE, 5234465 mN

Sample EF-09 is from the south face of the trench excavation (Fig. 8), within the lower half of the gravel that mantles the scarp, immediately beneath the fault plane on the footwall block. The footwall gravel appears to be identical to that on the hanging wall. The age of the EF-09 gravel provides a way to test this hypothesis.

Subgravel Soil at Trench Locality, HB (Sample EF-07)

55G, 446654 mE, 5234465 mN

Sample EF-07 is from the south face of the trench excavation (Fig. 8) from within a lens of brown medium-grained silty sand. The lens is beneath the gravel mantling the scarp in the hanging-wall block and is partly intercalated with the gravels. We suggest that the unit may have been ripped up from the underlying silty sand strata and redeposited. Hence, the age of the sampled material provides a maximum time bound for the deposition of the overlying gravel sheet.

Subgravel Soil at Trench Locality, HB (Sample EF-10)

55G, 446654 mE, 5234465 mN

Sample EF-10 is from the south face of the trench excavation (Fig. 8), from within the dark-brown organic-rich sediment that underlies the gravel. The sample was taken from the hanging-wall block above sample EF-09. Samples EF-09 and EF-10,

which are on either side of the main MRE fault strand, therefore provide a test on the nature of faulting. Reverse motion should juxtapose older sediment above younger sediment.

**Colluvial Fan Derived from Terrace 1, FB (Sample EF-03)
55G, 446673 mE, 5234190 mN**

Sample EF-03 is from a small hand-excavated pit dug into the upper surface of a localized colluvial fan shed off terrace 1 onto the footwall block fan (Figs. 6C and 7). The fan mantles the fault scarp and is not displaced by faulting, so this material must postdate the MRE.

The stratigraphy at the sample site is composed of an upper 210-mm-thick layer of dark-brown peaty soil overlying a 110-mm-thick layer of gravelly coarse sand. This sandy layer underlies the surface of the colluvial fan. The sample was taken from this layer. The sand is underlain by a third unit, which is a brown gravelly clay that extends to the base of the pit (~450 mm). The gravel clasts are identical to those on terrace 1. Leveling data (Figs. 6C and 7) suggest that the gravelly clay is also part of the colluvial fan.

Footwall Block Fluvial Fan, FB (Sample EF-12)

55G, 446739 mE, 5234182 mN

Sample EF-12 is from a small hand-excavated pit in the main fluvial fan, ~50 m east of the fault scarp (Figs. 6C and 7). Because the fan dips moderately to the west, it was judged that sediment from this location would not be contaminated by material derived from the upthrown block.

The stratigraphy at the site of sampling is composed of an upper 250-mm-thick layer of peaty soil rich in roots that overlies sandy gravel, which extends beneath the soil pit at 500 mm depth. The gravel is poorly sorted and contains angular and subrounded clasts that range from 5 to 150 mm in size. Clasts are typically quartzite or vein quartz and appear to have undergone a similar amount of weathering to those on terrace 1 (see EF-11 description). The age of this sample will give an indication of the age structure of the footwall fluvial fan.

Terrace 2, HB (Sample EF-17)

55G, 446649 mE, 5234046 mN

Sample EF-17 was taken from a small hand-excavated pit in the upper surface of terrace 2 along the line of the “Three terrace” traverse (Figs. 6C and 7C). The stratigraphy at the sampled location consists of (1) an upper 230-mm-thick peaty soil horizon, overlying (2) a 100 mm layer of well-sorted fine sandy loam, and (3) >100 mm of sandy/clayey gravel (sandy near the upper contact, becoming more clayey with depth). The clasts are composed of quartzite ~10 mm in diameter in the upper 50–70 mm of the layer, grading to cobbles as much as 200 mm in diameter near the base of the pit (e.g., Fig. 3F). The gravel clasts within the pit, and elsewhere on terrace 2, have similar competence as those on

terrace 1. The burial age derived from this sediment provides a maximum bound on the time of initial uplift of terrace 2 above the footwall fan level, during the penultimate event (PE1).

Terrace 3, HB (Sample EF-06)
55G, 446618 mE, 5234021 mN

Sample EF-06 is from a small hand-excavated pit in the upper surface of a remnant (outlier) of terrace 3 along the line of the “Three terrace” traverse (Figs. 6C and 7C). The stratigraphy at the location of the sample is composed of 250 mm of peaty soil that overlies a gravelly medium sand that extends beneath the 400 mm depth of the pit. The gravel and cobbles appear much more weathered on terrace 3 than on terraces 1 and 2. In many instances, they will crumble when struck with a hammer, or even when handled. The clast composition and angularity appear to be similar to that on other terraces, however, implying a similar source region and transport distance. The sample was taken from the gravel layer. The age derived from this sample provides a maximum bound on the time of initial uplift of terrace 3 above the footwall fan level, during an older penultimate event (PE2).

Fault-Bounded Pond, Colluvial Deposit Derived from MRE Scarp, FB (Sample EF-15)
55G, 446836 mE, 5242629 mN

Sample EF-15 is from the small fault-bounded lake north of Harlequin Hill (Fig. 5). Clayey to sandy gravel was retrieved from the borehole closest to the scarp (borehole 2, 5 m east of the scarp; Fig. 10), from within a unit that overlies the prelake fluvial fan deposits and underlies lake sand and mud. The gravel clasts are angular to subrounded quartzite and platy phyllite. This unit is interpreted to be colluvium shed off the fault scarp or terrace 1 after the MRE. The age of deposition of the sample therefore postdates the MRE.

A soil pit was excavated into the toe of the scarp (terrace 1) adjacent to borehole 2 to see if the materials exposed matched those interpreted to be prelake fluvial fan sediments in the boreholes. The stratigraphy exposed in the pit consists of an upper 270-mm-thick layer of dark-brown organic-rich silty clay at the surface underlain by a light-brown gravelly clay. The clasts consist of dominant quartzite and phyllite to a diameter of 40 mm, very similar to that seen in the boreholes.

Fault-Bounded Pond, Sand-Organics Transition, FB (Sample EF-14)
55G, 446858 mE, 5242621 mN

Sample EF-14 is from the small fault-bounded lake located near the center of the fault’s length. Clayey sand was retrieved from the borehole 25 m east of the scarp base (borehole 3; Fig. 10) from within a sandy unit immediately underlying organic muds. This unit is interpreted to be lacustrine in origin, and it provides

the potential to date the transition from sandy to organic sedimentation within the lake.

APPENDIX 2. OSL PROCEDURES AND TECHNIQUES

Background

Methods of dating sediment by stimulated luminescence rely on the net redistribution of charge that takes place when ionizing radiation interacts with an insulating crystal lattice, such as quartz (Aitken, 1977, 1998). When crystals in a sample are exposed to natural radionuclides in the environment, some electrons move out to the outer shells of atoms, where they may accumulate in meta-stable traps within the crystal lattice. As the net charge redistribution continues for the duration of the ionizing exposure (i.e., as long as sediment remains buried), the amount of trapped charge increases in proportion to both the duration and intensity of radiation exposure. Optical stimulation in the laboratory releases the stored electrons, emitting energy as light (luminescence).

Optical energy can stimulate luminescence and, since the mid-1980s, optically stimulated luminescence (OSL) has been used to date crystals in sediment (Huntley et al., 1985). Optical dating provides a measure of time since sediment was last exposed to sunlight. Exposure at the surface may bleach (partial) or reset (total) the OSL signal of a sediment. Subsequent burial by further sedimentation causes the grains to accumulate trapped charges (measured as the radiation dose) from ionizing radioelements in the deposit, mainly from U and Th decay chains and ^{40}K , and cosmic rays. This accumulated energy is known as the paleodose or equivalent dose and is proportional to the age of the sample. Crystals are exposed to light in the laboratory to release their store of trapped energy. The age of the sample is the accumulated dose divided by the dose rate.

$$\text{Age (time)} = \frac{\text{Dose (Radiation energy)}}{\text{Dose rate (Radiation energy/time)}}.$$

Technique

We collected samples for OSL dating by hammering 40-mm-diameter stainless-steel tubes into freshly cleaned sediment on vertical faces. Polymimetic samples were prepared under subdued, red light using standard procedures (Galbraith et al., 1999). The 90–125 μm quartz fraction was retained for dating.

Equivalent doses were calculated using a single-aliquot regenerative dose (SAR) protocol (Murray and Roberts, 1998; Galbraith et al., 1999; Murray and Wintle, 2000). Small aliquots of ~100–200 grains were preheated at either 240 or 260 °C for 10 s and optically stimulated for 100 s at 125 °C by blue (470 nm) light from light-emitting diode (LED) arrays attached to an automated RISØ TL-DA-15 apparatus. Luminescence was detected using a Thorn-EMI 9235QB15 p.m. tube with a 7.5 mm Hoya U-340 filter. The grains were then given applied doses using a

calibrated $^{90}\text{Sr}/^{90}\text{Y}$ beta-source and restimulated to record their regenerative OSL signals. Samples were given test doses of 2 Gy after each optical stimulation to monitor OSL sensitivity changes in the quartz crystals between the natural and regenerative cycles.

OSL signals were integrated over the first 4.8 s period of illumination, with the mean signal from the final 20 s of illumination converted to the equivalent number of channels over 4.8 s and subtracted as background using Analyst version 2.12 software (Duller, 1999). The OSL data were corrected for any sensitivity changes, and dose-response curves were constructed using a minimum of six regenerative dose points. The equivalent dose was obtained from the intercept of the regenerated dose-response curve with the natural luminescence intensity.

Frequency distributions of equivalent dose estimates from single aliquots were typically skewed by older equivalent doses. This suggests that most of the samples contained substantial populations of grains that had been inadequately exposed to sunlight prior to the last depositional event. Ages were generated using the weighted mean (central age; Galbraith et al., 1999) equivalent dose of the youngest quartile of aliquots to minimize the effect of partially bleached grains.

Preheat tests produced flat plateaus over the range 160–300 °C, indicating negligible thermal transfer in all of the samples. Recuperation tests showed no significant radiative recombination. These experiments, including recycling tests using duplicate regenerations of known dose, confirmed the reproducibility of the laboratory-induced luminescence signals.

K, U, and Th concentrations were estimated by instrumental neutron activation analysis (INAA). These were converted to beta dose rates using the conversion factors of Adamiec and Aitken (1998) with a beta attenuation factor of 0.93 ± 0.03 (Mejdahl, 1979). Gamma dose rates were measured in the field for all except three samples using a portable spectrometer with NaI (TI) crystal and converted to dry values by oven-drying sediment from the sample location. Gamma dose rates were estimated from the INAA radionuclide concentrations for those samples lacking in situ gamma spectrometry. Alpha dose rates were assumed to be $0.03 \pm 0.01 \text{ mGy yr}^{-1}$, a conservative estimate based on measurements of Australian quartz elsewhere (e.g., Bowler et al., 2003).

Cosmic-ray dose rates were determined from established equations (Prescott and Hutton, 1994), allowing for sample depth, sediment density, and site altitude, latitude and longitude. Time-averaged moisture content of the sediments was estimated from the oven-dried weight of OSL sediment samples and used to correct attenuation by water (Aitken, 1998). Present-day field water contents, which varied from 12.5% to 40% (Table 1), are considered representative of long-term averages.

REFERENCES CITED

- Adamiec, G., and Aitken, M.J., 1998, Dose-rate conversion factors—Update: Ancient TL, v. 16, p. 37–50.
- Aitken, M.J., 1977, Thermoluminescence and the archaeologist: *Antiquity*, v. 51, p. 11–19.
- Aitken, M.J., 1998, An Introduction to Optical Dating: Oxford, Oxford University Press, 280 p.
- Balmer, J., and Corbett, E., 2001, The vegetation of the Lake Pedder area prior to flooding, in Sharples, C., ed., Lake Pedder: Values and Restoration: Centre for Environmental Studies, University of Tasmania, Occasional Paper 27, p. 67–86.
- Barrows, T.T., Stone, J.O., Fifield, L.K., and Cresswell, R.G., 2001, Late Pleistocene glaciation of the Kosciusko Massif, Snowy Mountains, Australia: Quaternary Research, v. 55, p. 179–189, doi:10.1006/qres.2001.2216.
- Barrows, T.T., Stone, J.O., Fifield, L.K., and Cresswell, R.G., 2002, The timing of the Last Glacial Maximum in Australia: Quaternary Science Reviews, v. 21, p. 159–173, doi:10.1016/S0277-3791(01)00109-3.
- Bowler, J.M., Johnston, H., Olley, J.M., Prescott, J.R., Roberts, R.G., Shawcross, W., and Spooner, N.A., 2003, New ages for human occupation and climatic change at Lake Mungo, Australia: *Nature*, v. 421, p. 837–840, doi:10.1038/nature01383.
- Brown, A.V., Calver, C.R., Corbett, K.D., Forsyth, S.M., Goscombe, B.A., Green, G.R., McClenaghan, M.P., Pemberton, J., and Seymour, D.B., compilers, 1995, Geology of Southwest Tasmania: Geological Atlas 1:250,000 Digital Series: Hobart, Tasmanian Geological Survey, scale 1:250,000.
- Burbank, D.W., and Anderson, R.S., 2000, Tectonic Geomorphology: Oxford, UK, Blackwell Science Inc., 288 p.
- Calver, C.R., Turner, N.J., McClenaghan, M.P., and McClenaghan, J., 1990, Pedder: Geological Survey Explanatory Report, Sheet 80: Hobart, Tasmanian Department of Resources and Energy, 105 p.
- Carey, S.W., and Newstead, G., 1960, Tasmania University Seismic Net: Geology Department, University of Tasmania, Publication 84, p. 9–14.
- Clark, D.J., and Bodorkos, S., 2004, Fracture systems in granite pavements of the eastern Pilbara craton, Western Australia: Indicators of neotectonic activity: *Australian Journal of Earth Sciences*, v. 51, p. 831–846, doi:10.1111/j.1400-0952.2004.01088.x.
- Clark, D.J., and McCue, K., 2003, Australian palaeoseismology: Towards a better basis for seismic hazard estimation: *Annals of Geophysics*, v. 46, p. 1087–1105.
- Colhoun, E., 2003, Antipodal terrestrial deglacial events from Ireland and Tasmania (paper 83-1), in 16th International Quaternary Association Congress Program with Abstracts: Reno, Nevada, p. 221. Available at http://gsa.confex.com/gsa/inqu/finalprogram/abstract_54762.htm (accessed 31 May 2011).
- Colhoun, E.A., and Fitzsimons, S.J., 1990, Late Cainozoic glaciation in western Tasmania, Australia: Quaternary Science Reviews, v. 9, p. 199–216, doi:10.1016/0277-3791(90)90018-6.
- Crone, A.J., and Luza, K.V., 1990, Style and timing of Holocene surface faulting on the Meers fault, southwestern Oklahoma: *Geological Society of America Bulletin*, v. 102, p. 1–17, doi:10.1130/0016-7606(1990)102<0001:SATHS>2.3.CO;2.
- Crone, A.J., Machette, M.N., and Bowman, J.R., 1992, Geologic Investigations of the 1988 Tenant Creek, Australia, Earthquakes—Implications for Paleoseismicity in Stable Continental Regions: U.S. Geological Survey Bulletin 2032-A, 51 p.
- Crone, A.J., Machette, M.N., and Bowman, J.R., 1997, Episodic nature of earthquake activity in stable continental regions revealed by paleoseismicity studies of Australian and North American Quaternary faults: *Australian Journal of Earth Sciences*, v. 44, p. 203–214, doi:10.1080/08120099708728304.
- Crone, A.J., de Martini, P.M., Machette, M.N., Okumura, K., and Prescott, J.R., 2003, Paleoseismicity of aseismic Quaternary faults in Australia: Implications for fault behaviour in stable continental regions: *Bulletin of the Seismological Society of America*, v. 93, p. 1913–1934, doi:10.1785/0120000094.
- Duller, G.A.T., 1999, Analyst Version 2.12: Aberystwyth, UK, Luminescence Laboratory, University of Wales.
- Fink, D., and Williams, P., 2003, Timing of the Last Glacial Maximum in Fiordland, New Zealand—But was it the last advance? (paper 5-1), in 16th International Quaternary Association Congress Program with Abstracts: Reno, Nevada, p. 74. Available at http://gsa.confex.com/gsa/inqu/finalprogram/abstract_54455.htm (accessed 31 May 2011).
- Galbraith, R.F., Roberts, R.G., Laslett, G.M., Yoshida, H., and Olley, J.M., 1999, Optical dating of single and multiple grains of quartz from Jimmum rock shelter, northern Australia: Part I. Experimental design and statistical models: *Archaeometry*, v. 41, p. 339–364, doi:10.1111/j.1475-4754.1999.tb00987.x.

- Hemphill, H.M.A., and Weldon, R.J.I., 1999, Estimating prehistoric earthquake magnitude from point measurements of surface rupture: *Bulletin of the Seismological Society of America*, v. 89, p. 1264–1279.
- Huntley, D.J., Godfrey-Smith, D.I., and Thewalt, M.L.W., 1985, Optical dating of sediments: *Nature*, v. 313, p. 105–107, doi:10.1038/313105a0.
- International Atomic Energy Agency (IAEA), 1991, Earthquakes and Associated Topics in Relation to Nuclear Power Plant Siting: International Atomic Energy Agency Safety Series 50-SG-S1 Revision 1, Code of Practice, 70 p.
- Johnson, A.C., Coppersmith, K.J., Kanter, L.R., and Cornell, C.A., 1994, The Earthquakes of Stable Continental Regions: *Electric Power Research Institute Report TR102261V1*, 309 p.
- Kiernan, K., 1985, Late Cainozoic Glaciation and Mountain Geomorphology in the Central Highlands of Tasmania [Ph.D. thesis]: Hobart, Department of Geography, University of Tasmania, 2 vols., 557 p.
- Kiernan, K., 1990, The alpine geomorphology of the Mt. Anne Massif, south-western Tasmania: *The Australian Geographer*, v. 21, p. 113–125, doi:10.1080/00049189008703008.
- Kiernan, K., 2001, The geomorphology and geoconservation significance of Lake Pedder, in Sharples, C., ed., *Lake Pedder: Values and Restoration*: Centre for Environmental Studies, University of Tasmania, Occasional Paper 27, p. 13–50.
- Kiernan, K., Fifield, L., and Chappell, J., 2004, Cosmogenic nuclide ages for Last Glacial Maximum moraine at Schnells Ridge, southwest Tasmania: *Quaternary Research*, v. 61, p. 335–338, doi:10.1016/j.yqres.2004.02.004.
- Machette, M.N., 1998, Contrasts between short- and long-term records of seismicity in the Rio Grande Rift—Important implications for seismic hazard assessments in areas of slow extension, in Lund, W.R., ed., *Proceedings of the Basin and Range Province Seismic-Hazards Summit*: Utah Geological Survey Miscellaneous Publication 98, p. 84–95.
- Machette, M.N., 2000, Active, capable, and potentially active faults—A paleoseismic perspective: *Journal of Geodynamics*, v. 29, p. 387–392, doi:10.1016/S0264-3707(99)00060-5.
- McCue, K.F., 1990, Australia's large earthquakes and Recent fault scarps: *Journal of Structural Geology*, v. 12, p. 761–766, doi:10.1016/0191-8141(90)90087-F.
- McCue, K.F., Van Dissen, R., Gibson, G., Jensen, V., and Boreham, B., 2003, The Lake Edgar fault—An active fault in southwest Tasmania, Australia, with repeated displacement in the Quaternary: *Annals of Geophysics*, v. 46, p. 1107–1117.
- Mejdahl, V., 1979, Thermoluminescence dating: Beta-dose attenuation in quartz grains: *Archaeometry*, v. 21, p. 61–72, doi:10.1111/j.1475-4754.1979.tb00241.x.
- Michael-Leiba, M.O., and Gaull, B.A., 1989, Probabilistic earthquake risk maps of Tasmania: *BMR Journal of Australian Geology and Geophysics*, v. 11, p. 81–87.
- Miller, G.H., Magee, J.W., and Jull, A.J.T., 1997, Low-altitude cooling in the Southern Hemisphere from amino-acid racemization in emu eggshells: *Nature*, v. 385, p. 241–244, doi:10.1038/385241a0.
- Murray, A.S., and Roberts, R.G., 1998, Measurement of the equivalent dose in quartz using a regenerative-dose single-aliquot protocol: *Radiation Measurements*, v. 29, p. 503–515, doi:10.1016/S1350-4487(98)00044-4.
- Murray, A.S., and Wintle, A.G., 2000, Luminescence dating of quartz using an improved single-aliquot regenerative-dose protocol: *Radiation Measurements*, v. 32, p. 57–73, doi:10.1016/S1350-4487(99)00253-X.
- Olley, J.M., Pietsch, T., and Roberts, R.G., 2004, Optical dating of Holocene sediments from a variety of geomorphic settings using single grains of quartz: *Geomorphology*, v. 60, p. 337–358.
- Prescott, J.R., and Hutton, J.T., 1994, Cosmic ray contributions to dose rates for luminescence and ESR dating: Large depths and long-term time variations: *Radiation Measurements*, v. 23, p. 497–500, doi:10.1016/1350-4487(94)90086-8.
- Roberts, G.T., Cole, B.A., and Barnett, R.H.W., 1975, Engineering geology of Scotts Peak dam and adjacent reservoir: Watertightness: *Australian Geomechanics Journal*, v. G5, p. 39–45.
- Sandiford, M., 2003a, Neotectonics of southeastern Australia: Linking the Quaternary faulting record with seismicity and in situ stress, in Hillis, R.R., and Muller, D., eds., *Evolution and Dynamics of the Australian Plate*: Geological Society of Australia Special Publication 22, p. 101–113.
- Sandiford, M., 2003b, Geomorphic constraints on the late Neogene tectonics of the Otway Ranges: *Australian Journal of Earth Sciences*, v. 50, p. 69–80, doi:10.1046/j.1440-0952.2003.00973.x.
- Schwartz, D.P., and Coppersmith, K.J., 1984, Fault behaviour and characteristic earthquakes: Examples from the Wasatch and San Andreas fault zones: *Journal of Geophysical Research*, v. 89, no. B7, p. 5681–5698, doi:10.1029/JB089IB07p05681.
- Seymour, D.B., and Calver, C.R., 1995, Stratotectonic Elements Map: Tasmanian Geological Survey, Tasmania Development and Resources, and Australian Geological Survey Organisation, scale 1:500,000, 1 sheet.
- Shirley, J.E., 1980, Tasmanian seismicity—Natural and reservoir-induced: *Bulletin of the Seismological Society of America*, v. 70, p. 2203–2220.
- Turner, N.J., Calver, C.R., McClenaghan, M.P., McLenaghan, J., Brown, A.V., Lennox, P.G., Boutler, C.A., and Godfrey, N.H.H., 1985, Pedder: Geological Atlas, 1:50,000 Series Sheet 8112 S (80): Hobart, Geological Survey of Tasmania, Department of Mines, scale 1:50,000.
- U.S. Nuclear Regulatory Commission (USNRC), 1996, Geologic and Seismic Siting Factors for Nuclear Power Plants: U.S. Nuclear Regulatory Commission, Section 100.23 10 CFR Part 100; available at <http://www.nrc.gov/reading-rm/doc-collections/cfr/part100/part100-0023.html> (accessed 31 May 2011).
- Wells, D.L., and Coppersmith, K.J., 1994, New empirical relationships among magnitude, rupture length, rupture width, rupture area, and surface displacement: *Bulletin of the Seismological Society of America*, v. 84, p. 974–1002.
- Williams, P.W., 1996, A 230 ka record of glacial and interglacial events from Aurora Cave, Fiordland, New Zealand: *New Zealand Journal of Geology and Geophysics*, v. 39, p. 225–241, doi:10.1080/00288306.1996.9514707.

MANUSCRIPT ACCEPTED BY THE SOCIETY 7 DECEMBER 2010

